Journal of Instrumentation

The evaporative cooling system for the ATLAS inner detector

To cite this article: D Attree *et al* 2008 *JINST* **3** P07003

PUBLISHED BY INSTITUTE OF PHYSICS PUBLISHING AND SISSA

RECEIVED: *April 28, 2008*
ACCEPTED: *June 30, 2008*
PUBLISHED: *July 15, 2008*

The evaporative cooling system for the ATLAS inner detector

D. Attree,[a] B. Anderson,[a] E.C. Anderssen,[b] V. Akhnazarov,[c] R.J. Apsimon,[d] P. Barclay,[d] L.E. Batchelor,[d] R.L. Bates,[e] M. Battistin,[f] J. Bendotti,[f] S. Berry,[f] A. Bitadze,[f] J.P. Bizzel,[f] P. Bonneau,[f] M. Bosteels,[f] J.M. Butterworth,[a] S. Butterworth,[d] A.A. Carter,[g] J.R. Carter,[h] A. Catinaccio,[f] F. Corbaz,[f] H.O. Danielsson,[f] E. Danilevich,[i] N. Dixon,[f] S.D. Dixon,[j] F. Doherty,[e] O. Dorholt,[k] M. Doubrava,[l] K. Egorov,[n] K. Einsweiler,[b] A.C. Falou,[o] P. Feraudet,[f] P. Ferrari,[f] K. Fowler,[p] J.T. Fraser,[a] R.S. French,[j] M. Galuska,[l] F. Gannaway,[g] G. Gariano,[q] M.D. Gibson,[d] M. Gilchriese,[b] D. Giugni,[r] J. Godlewski,[f] I. Gousakov,[s] B. Gorski,[t] G.D. Hallewell,[u] N. Hartman,[b] R.J. Hawkings,[f] S.J. Haywood,[d] N.P. Hessey,[v] I. Ilyashenko,[m] S. Infante,[f] J.N. Jackson,[w] T.J. Jones,[w] J. Kaplon,[f] S. Katunin,[i] S. Lindsay,[w] L. Luisa,[x] N. Massol,[y] F. McEwan,[e] S.J. McMahon,[d] C. Menot,[f] J. Mistry,[g] J. Morris,[g] D.M. Muskett,[w] K. Nagai,[g] A. Nichols,[d] R. Nicholson,[j] R.B. Nickerson,[z] S.L. Nielsen,[k] P.E. Nordahl,[k] M. Olcese,[q*] M. Parodi,[q] F. Perez-Gomez,[f] H. Pernegger,[f] E. Perrin,[aa] L.P. Rossi,[q] A. Rovani,[q] E. Ruscino,[q] H. Sandaker,[ab] A. Smith,[b] V. Sopko,[l] S. Stapnes,[k] M. Stodulski,[ac] J. Tarrant,[d] J. Thadome,[ad] D. Tovey,[j] M. Turala,[ac] M. Tyndel,[d] V. Vacek,[l] E. van der Kraaij,[v] G.H.A. Viehhauser,[z] E. Vigeolas,[u] P.S. Wells,[f] S. Wenig[f] and P. Werneke[v]

[a] *University College London, Department of Physics and Astronomy, Gower Street, London, WC1E 6BT, United Kingdom*
[b] *Lawrence Berkeley National Laboratory and University of California, Physics Division, MS50B-6227, 1 Cyclotron Road, Berkeley, CA 94720, United States of America*
[c] *TRIUMF, 4004 Wesbrook Mall, Vancouver, B.C. V6T 2A3, Canada*
[d] *Rutherford Appleton Laboratory, Science and Technology Facilities Council, Harwell Science and Innovation Campus, Didcot OX11 0QX, United Kingdom*
[e] *University of Glasgow, Department of Physics and Astronomy, Glasgow G12 8QQ, United Kingdom*
[f] *CERN, CH - 1211 Geneva 23, Switzerland*
[g] *Department of Physics, Queen Mary, University of London, Mile End Road, London E1 4NS, United Kingdom*
[h] *Cavendish Laboratory, University of Cambridge, J J Thomson Avenue, Cambridge CB3 0HE, United Kingdom*
[i] *Petersburg Nuclear Physics Institute, RU - 188 300 Gatchina, Russia*
[j] *University of Sheffield, Department of Physics & Astronomy, Hounsfield Road, Sheffield S3, 7RH, United Kingdom*
[k] *Department of Physics, University of Oslo, Blindern, NO - 0316 Oslo 3, Norway*

2008 JINST 3 P07003

[l] *Czech Technical University in Prague, Department of Applied Physics, Technická 4, CZ - 166 07 Praha 6, Czech Republic*
[m] *Ioffe Physical-Technical Institute, St.Petersburg, 194021, Russia*
[n] *Indiana University, Department of Physics, Swain Hall West, Room 117, 727 East Third St., Bloomington, IN 47405-7105, United States of America*
[o] *LAL, Univ. Paris-Sud, IN2P3/CNRS, Orsay, France*
[p] *University of California Santa Cruz, Santa Cruz Institute for Particle Physics (SCIPP), Santa Cruz, CA 95064, United States of America*
[q] *INFN Genova and Università di Genova, Dipartimento di Fisica, via Dodecaneso 33, IT - 16146 Genova, Italy*
[r] *INFN Milano and Università di Milano, Dipartimento di Fisica, via Celoria 16, IT – 20133 Milano, Italy*
[s] *Joint Institute for Nuclear Research, JINR Dubna, RU - 141 980 Moscow Region, Russia*
[t] *Cracow University of Technology, ul. Warszawska 24, Cracow, Poland*
[u] *CPPM, Aix-Marseille Université, CNRS/IN2P3, Marseille, France*
[v] *Nikhef National Institute for Subatomic Physics, Kruislaan 409, P.O. Box 41882, NL – 1009 DB Amsterdam, Netherlands*
[w] *Oliver Lodge Laboratory, University of Liverpool, P.O. Box 147, Oxford Street, Liverpool L69 3BX, United Kingdom*
[x] *INFN Gruppo Collegato di Udine and Università di Udine, Dipartimento di Fisica, via delle Scienze 208, IT - 33100 Udine; INFN Gruppo Collegato di Udine and ICTP, Strada Costiera 11, IT - 34014 Trieste, Italy*
[y] *Laboratoire d'Annecy-le-Vieux de Physique des Particules LAPP, IN2P3/CNRS, Université de Savoie, France*
[z] *Department of Physics, Oxford University, Denys Wilkinson Building, Keble Road, Oxford OX1 3RH, United Kingdom*
[aa] *Université de Genève, Section de Physique, 24 rue Ernest Ansermet, CH - 1211 Geneve 4, Switzerland*
[ab] *University of Bergen, Department for Physics and Technology, Allegaten 55, NO – 5007 Bergen, Norway*
[ac] *The Henryk Niewodniczanski Institute of Nuclear Physics, Polish Academy of Sciences, ul. Radzikowskiego 152, PL - 31342 Krakow, Poland*
[ad] *Bergische Universitaet, Fachbereich C, Physik, Postfach 100127, Gauss-Strasse 20, DE-42097 Wuppertal, Germany*
E-mail: marco.olcese@cern.ch

ABSTRACT: This paper describes the evaporative system used to cool the silicon detector structures of the inner detector sub-detectors of the ATLAS experiment at the CERN Large Hadron Collider. The motivation for an evaporative system, its design and construction are discussed. In detail the particular requirements of the ATLAS inner detector, technical choices and the qualification and manufacture of final components are addressed. Finally results of initial operational tests are reported. Although the entire system described, the paper focuses on the on-detector aspects. Details of the evaporative cooling plant will be discussed elsewhere.

KEYWORDS: Particle tracking detectors; Detector cooling and thermo-stabilization.

*Corresponding author.

2008 JINST 3 P07003

Contents

2008 JINST 3 P07003

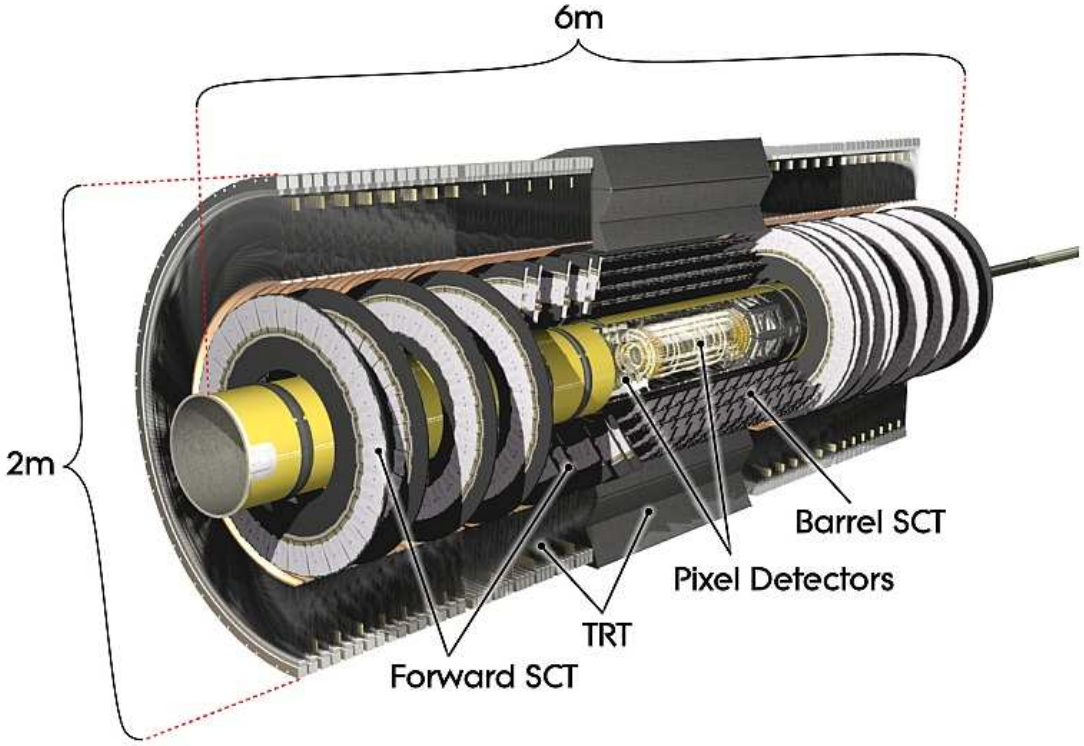

Figure 1. The Inner Tracker of the ATLAS experiment.

2008 JINST 3 P07003

1. Introduction

The ATLAS detector [1] is a multi-purpose detector currently being constructed at one of the four interaction points of the LHC [2] accelerator. The detector will study interaction products from proton-proton collisions with a 14 TeV centre-of-mass energy at a design luminosity of $10^{34}\,\mathrm{cm}^{-2}\mathrm{s}^{-1}$. The detector consists of three main sub-detector types, namely; trackers, calorimeters and muon chambers, centred on the interaction point. The central tracker, the Inner Detector (ID) [3], is situated inside a 2 T central superconducting solenoid magnet [4] (figure 1).

It consists of the silicon Pixel detector closest to the beam, surrounded by the SemiConductor Tracker (SCT) detector and the outer Transition Radiation Tracker (TRT). During the envisaged 10 years of operation the total particle fluence is expected to be of 2×10^{14} 1-MeV neutron equivalent cm^{-2} at the innermost layer of the SCT [3], resulting in a continuous degradation of the detectors, corresponding to an increase in device leakage currents. The inner most layer of the Pixel system experiences an even greater particle fluence equal to 2×10^{15} 1-MeV neutron equivalent cm^{-2} after 10 years of operation.

The Pixel system will provide 3 or 4 space points per track and will have a pseudorapidity, η, coverage up to 2.5. There are 1744 modules in the Pixel Detector for nearly 80 million channels in a cylinder 1.4 m long, 0.5 m in diameter centred on the interaction point. The barrel part of

the pixel detector consists of the 3 cylindrical layers made of 112 identical staves. Each stave is composed of 13 pixel modules. In the module there are 16 front-end (FE) chips. There are three disks on each side of the forward regions. One disk is made of 8 sectors, with 6 modules in each sector. Disk modules are identical to the barrel modules, except for the connecting cables. The FE chips are a major heat source (0.8 W/cm2) dissipating more than 15 kW into the detector volume. This heat is taken out via integrated cooling channels in the detector support elements: staves in the barrel region and Sectors in the forward region. The modules are not in direct contact with the cooling tube, but they are cooled indirectly by the highly thermal conductive carbon-based support structure which has the cooling tubes embedded into it [5].

The SCT will provide at least four space points per track and will have a pseudorapidity, η, coverage up to 2.5. To achieve this, the detector consists of one central barrel, where 2112 barrel modules have been mounted to cover the full outer surfaces of four cylinders, and one end-cap in each forward region, where the 1976 end-cap modules have been mounted on 18 disks. The barrel detector modules are all identical. The end-cap modules [6] have four different radial geometries, depending on their position relative to the collision centre. Again the SCT modules dissipate a significant amount of heat, more than 25 kW, which is removed via cooling loops mounted on to the SCT carbon fibre support structures. The thermal contact between the cooling tubes and the modules is provided by cooling blocks soldered on the cooling tubes and in direct contact with the module surface.

2. Requirements

The cooling capacity of the SCT and Pixel cooling system must be sufficient to remove the heat from the detector modules and maintain the silicon temperature at or below $-7\ ^{\circ}$C for the SCT [7] and $0\ ^{\circ}$C for the Pixel [8] to prevent reverse annealing of the silicon detectors. The thermal resistances in the silicon module, between the module and its mounting point on the cooling circuit and the heat transfer to the fluid imply a required coolant temperature of $-25\ ^{o}$C. The temperature gradient along the cooling structure has also to be as small as possible for ease of design and operation.

The required cooling capacity has to be obtained while introducing a minimal amount of extra material into the detector volume in order to minimize the production of secondary particles. As well as the material restrictions, (measured in radiation length), on the system, the fact that the cooling circuit is deep within the ATLAS experiment requires the physical size of inlet and outlet pipes and cooling system components to be as small as possible.

The entire SCT/Pixel systems will be inside a thermal enclosure flushed with dry nitrogen. The system must be thermally neutral with respect to the rest of the experiment. The fluid used in the cooling system must be non-corrosive, non-toxic, radiation hard and non-flammable.

The total heat load that must be removed is almost 60 kW. After irradiation the leakage currents of the silicon detectors increase by more than an order of magnitude and their operating bias voltage increases by more than a factor of 3. Therefore these devices only become a significant heat source after an irradiation exposure. Due to the low mass requirements of the detector systems the power cables are thin and therefore there are significant voltage drops across these. The low mass tapes and pixel cables contribute 4% of the total heat load inside the thermal shield.

2008 JINST 3 P07003

An evaporative cooling system has been chosen for the SCT and pixel detector. The main motivation for an evaporative cooling system over a mono-phase system are: the higher heat transfer coefficient between the cooling fluid and the cooling tubes, the smaller temperature gradients along long cooling channels, and the smaller size required for the cooling channels. The smaller size of the system and thus lower coolant mass flows is due to the larger cooling capacity per unit volume in an evaporative system due to the utilization of the latent heat of vaporization rather than a liquids specific heat capacity.

3. The overall system design and architecture

3.1 Basic functionality

The evaporative system's basic functionality is similar to that of a standard industrial direct expansion cooling system. The fluid is delivered in liquid phase at room temperature from the condenser to the capillaries located immediately before the detector structures. The fluid expands through the capillaries and then remains in saturation conditions (boiling) along the cooling circuit on the detector structures. A heater, located at the exhaust of each circuit of the detector structures evaporates the residual liquid and raises the temperature of the vapour above the cavern dew point.

The fluid in superheated vapour phase and at room temperature is brought back to the compressor and then to the condenser.

Recuperative heat exchangers between the inlet liquid (warm) and the return fluid (cold), situated inside the dry environment of the thermal enclosure, are implemented to increase the efficiency of the thermodynamic cycle, by decreasing the vapour quality at the inlet of the detector structures and hence the required flow.

The reference thermodynamic states and transformations of the system are shown on the phase diagram of figure 2. Note that point D' corresponds to the thermodynamic state of the inlet liquid before entering the ID volume: since the possible temperature increase (if any) from the distribution racks (point D) to the detector volume is unknown, it has been assumed, as worst case, a max design temperature of 35 °C. This possible warm up of the inlet liquid could come from inefficiencies of the cable cooling system in the narrow gaps where the evaporative system tubes are routed together with the power cables for more than 20 m before reaching the ID volume.

In figure 2 the benefit of the inlet liquid sub cooling produced by the recuperative heat exchanger is evident: an inlet liquid temperature of -15 °C, compared with the 21 °C in case of no sub-cooling, allows almost a doubling of the fraction of the exploited phase-change enthalpy of the fluid in the detector structures.

This allows a reduction of the required mass flow of about 50%, which has a dramatic impact on the size of the on-detector structures and the size and cost of the main plant and on the overall system performance.

The temperature in the detector structures is set by setting the boiling pressure of the fluid. This is done by means of dome loaded backpressure regulators (BPR) located at the end of the return tubes. The flow is set by changing the pressure of the inlet liquid by means of pressure regulator (PR) located at the beginning of the inlet tubes.

Another major benefit of this solution is the possibility of keeping, outside the dry gas environment of the Inner Detector, both supply and return transfer lines at ambient temperature, in

2008 JINST 3 P07003

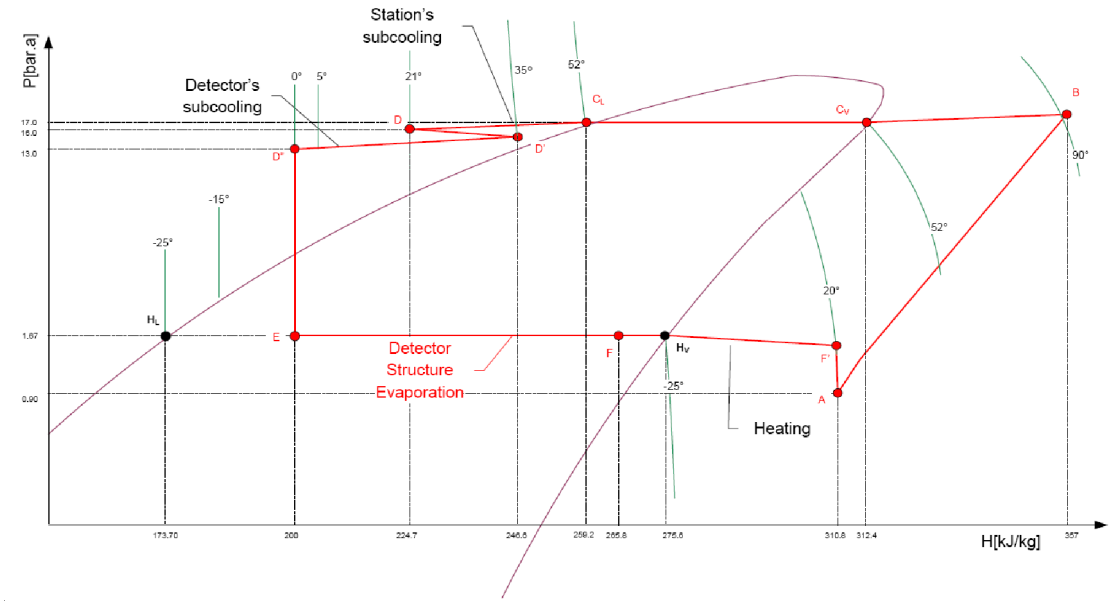

Figure 2. Phase diagram of the ATLAS Inner Detector evaporative cooling system.

liquid and gas phase respectively. Small mass flows and absence of insulation on the transfer lines translates into reduced space requirements along the pipe work to and from the Inner Detector. This is of paramount importance to improve the hermeticity of the ATLAS detector and its overall performance.

3.2 Fluid choice

The fluid choice is well documented in [9, 10].

The saturated n-type fluorocarbon refrigerants $C_nF_{(2n+2)}$ offer unique characteristics for the application in the cooling system of the ATLAS Inner Detector, these are: very good stability against irradiation, non-flammable, non-toxic, electrically insulator.

Various types of possible fluorocarbon candidates were investigated (C_3F_8, C_4F_{10}, C_3F_8/C_4F_{10} mixtures). Details of some of the physical properties of two possible refrigerant candidates are given in table 1.

After extensive tests C_3F_8 was chosen as the refrigerant for the ID[1] because:

- It shows the highest heat transfer coefficients
- It has a low saturated vapour pressure at the minimum operating temperature of -25 °C, which is still above the atmospheric pressure (this implies no air ingress from the environment)
- It gives lower pressure drops in the vapour phase, thus allowing for a reduced return tube size, which is critical for the ID services.

[1]Current supplier: ASTOR – St. Petersburg; minimum fluid purity requested: 99,96

2008 JINST 3 P07003

Table 1. Physical properties at $-15°C$ of two possible refrigerant candidates.

Refrigerant	Latent heat	Vapour volume per cm^3 of liquid	Vapour pressure
	[J/g]	[cm^3]	[bar_a]
C_4F_{10}	101.1	242.6	0.58
C_3F_8	97.0	71.4	2.46

C_2F_6 fluid is another possible candidate because of its much lower saturation temperature at atmospheric pressure. This property would allow to gain more headroom on the pressure drop budget over the return lines, which is critical in some cases with the present design as it is explained later, and potentially to run the detector at lower temperature.

However the major drawback of pure C_2F_6 is the much higher saturation pressure at room temperature (about 4 times the C_3F_8 saturation pressure). In case of failure of the fluid recovery system the detector structures would be potentially exposed to a pressure exceeding the design pressure of the current on-detector structures. This is the reason why the C_2F_6 is being considered as a possible alternative only in the context of the ID upgrade [11].

3.3 Overall system architecture

The ID evaporative system is a distributed system consisting of three main areas (figure 3):

- A main plant with the compressors, condenser and main system control located in the USA15 service cavern of the ATLAS experiment,
- A main fluid distribution system including the pipe work from the main plant and the 4 distribution racks located about 150 m away on the access platforms around the experiment in the main UX cavern.

An on-detector distribution system connecting the distribution racks to the ID detector and consisting of 204 individual circuits.

The segmentation of the detector cooling structures in terms of independent cooling circuits is maintained all the way out up to the distribution racks where the fluid control devices of each circuit are located: one pressure regulator and one backpressure regulator per circuit.

3.3.1 Pressure specifications

The critical requirement of the evaporative system is to be able to reach and maintain a stable operating temperature in the detector structures at the maximum power load equal to or less than -25 °C. This temperature is specified at the exhaust of the detector structures and corresponds to an absolute pressure of 1.67 bar absolute.

This requirement accounts for the thermal impedance between the coolant and the silicon modules and the pressure drops along the on-detector cooling channels.

The maximum temperature gradient between the silicon modules and the coolant came out of a long design optimization process of the sensor support structures as a trade off between the minimal mass requirement and the operational limits of the fluorocarbon-based evaporative cooling system [12].

2008 JINST 3 P07003

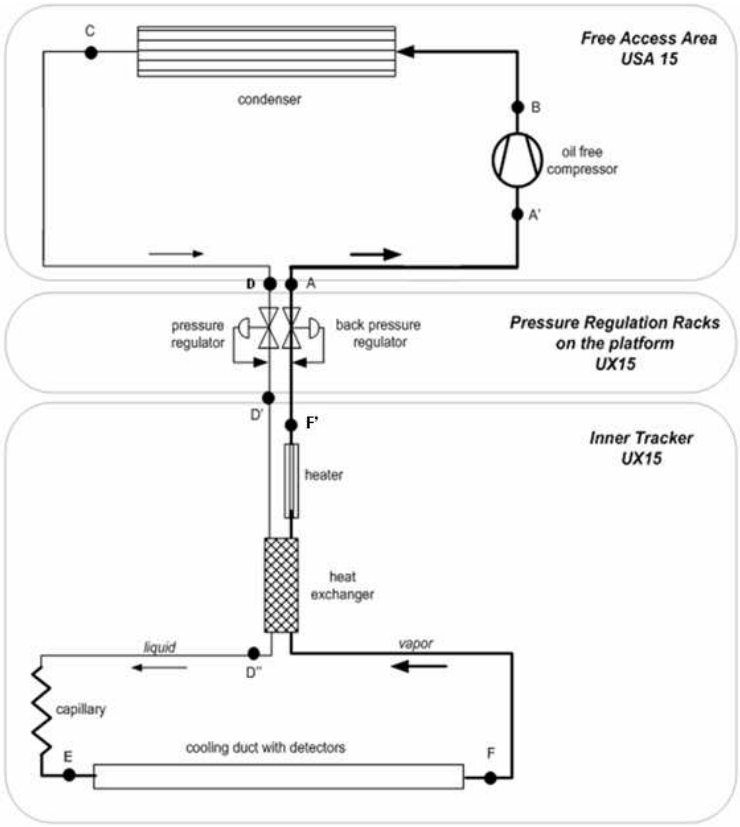

Figure 3. Schematic diagram of the evaporative system.

The pressure drop budget over the detector structure is not discussed here since it is a specific requirement of each subdetector. It is clear that this budget has to be as small as possible to minimize the fluid temperature changes along the detector structures. This maximum pressure requirement at the detector structures and the minimum possible input pressure of the compressors at full load set the available pressure drop budget for the vapour return lines from the detector to the compressor. This budget is 770 mbar, about 50% of which (350 mbar) is assigned as the budget for the on-detector part of the return tubes (from the detector to the distribution racks).

A 350 mbar pressure drop budget is an important constraint for the design of such a complex and tortuous pipe work, including heater and heat exchangers, which is also subject to severe space and material limitations especially inside the ID volume.

Therefore, the pressure drop budget on the exhaust tubes has been one of the key parameters driving the segmentation of the system (max number of circuits that can be run in parallel on a common exhaust tube).

The pressure drop budget of the inlet lines from the pressure regulators to the inlet of the capillaries is driven by the minimum pressure at the condenser and the minimum pressure before the capillaries, which has to be always above the saturation point to avoid vapour formation in the inlet tubes. The pressure drop budget of the inlet tubes is less critical then for the exhaust and was set to 1 bar.

The nominal design pressures of the evaporative cooling circuits are given in table 2.

2008 JINST 3 P07003

Table 2. Design pressure during normal operation at full power in the evaporative circuit (bar absolute).

Outlet of compressor	**Outlet of PR**	**Inlet capillary (min)**	**Outlet capillary**	**Detector structures (saturation at T = −25 °C)**	**Inlet of BPR**	**Inlet to the compressor**
17	14–15	13	1.67	1.67	1.3	0.9

The inlet pressure to the compressor is a function of the number of compressors working in parallel. The nominal 0.9 bar absolute inlet pressure should be achieved with 6 compressors in parallel. The main plant could host up to 7 compressors which would allow the input pressure to the compressor to be decreased down to 0.8 bar absolute, thus gaining more headroom for the pressure drops on the exhaust tubes from the detector to the distribution racks, which are critical, as discussed earlier.

3.3.2 Main plant and distribution racks

The evaporative cooling system circulating fluorocarbon C_3F_8 in closed loop has been designed to guarantee a total cooling capacity of 70 kW at a target temperature on the detector structures of -25 °C and supply a global mass flow rate of 1130 g/s.

The four quadrants of ATLAS Inner Detector are fed by 4 distribution racks installed on levels 1 and 7 of both sides of the ATLAS experiment (figure 4). Each rack is organized into an inlet and an outlet region and manages 51 circuits.

In each rack the distribution of the fluid is handled by 7 horizontal sub-manifolds connected to two main manifolds one for the inlet and one for the return.

There is one PR[2] and one BPR[3] for each circuit.

Each rack's main manifold is connected to the main manifold of the cooling station with an independent pipe, so there are 4 liquid lines and 4 vapour lines connecting the cooling station with the four distribution racks, allowing for an independent management of each distribution rack.

In USA15 Service cavern there is an area reserved to the main cooling station (shown in figure 5 and figure 6).

Up to a maximum of seven identical two-stage oil free compressors[4] work in parallel to compress the gas from 800 mbar absolute at the main return manifold to 17 bar absolute at their outputs. The electrical motor is magnetically coupled to the compressor. Six of these compressors are set to operate by an on/off valve. Only the seventh compressor has a by-pass line allowing for fine tuning (0–100%) of the flow-rate.

The control algorithm sets the number of on/off compressors in operation and tune the seventh compressor in order to maintain a constant pressure at the compressor inlet manifold.

After the compression phase the gas is condensed inside a mixed water plate heat exchanger. Water circulation inside the heat exchanger is regulated to maintain a constant condensation pressure.

[2]TESCOM: model 26-2301

[3]TESCOM: model 44-2200

[4]HAUG, model QTOGX 160/80 LM

2008 JINST 3 P07003

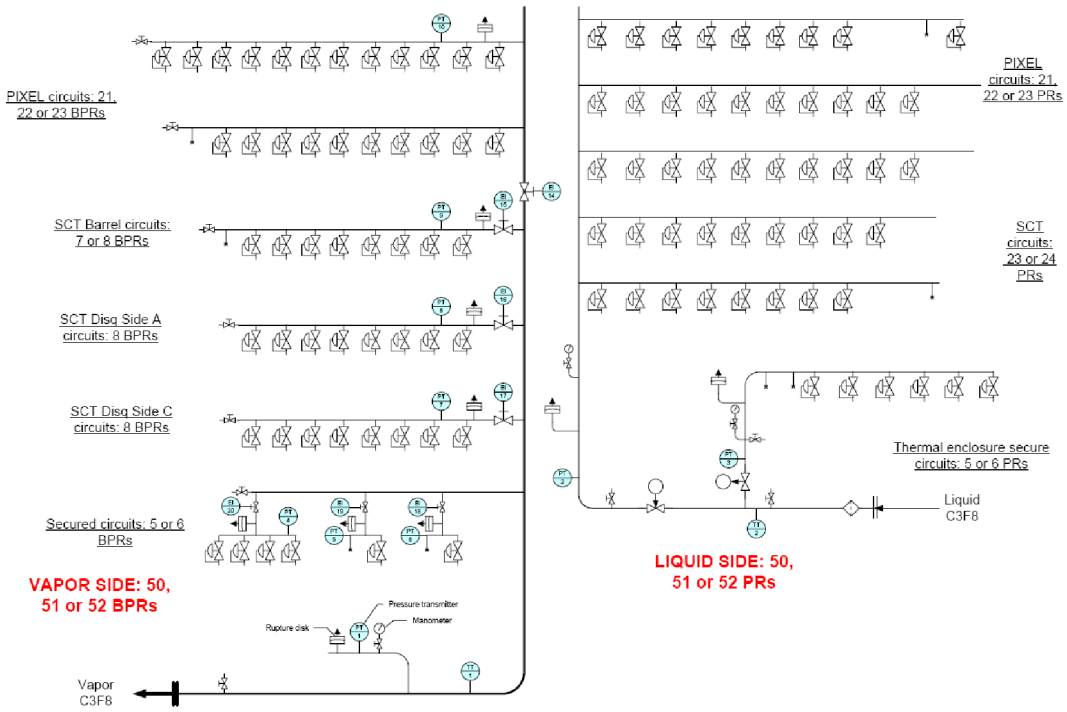

Figure 4. The layout of the distribution rack.

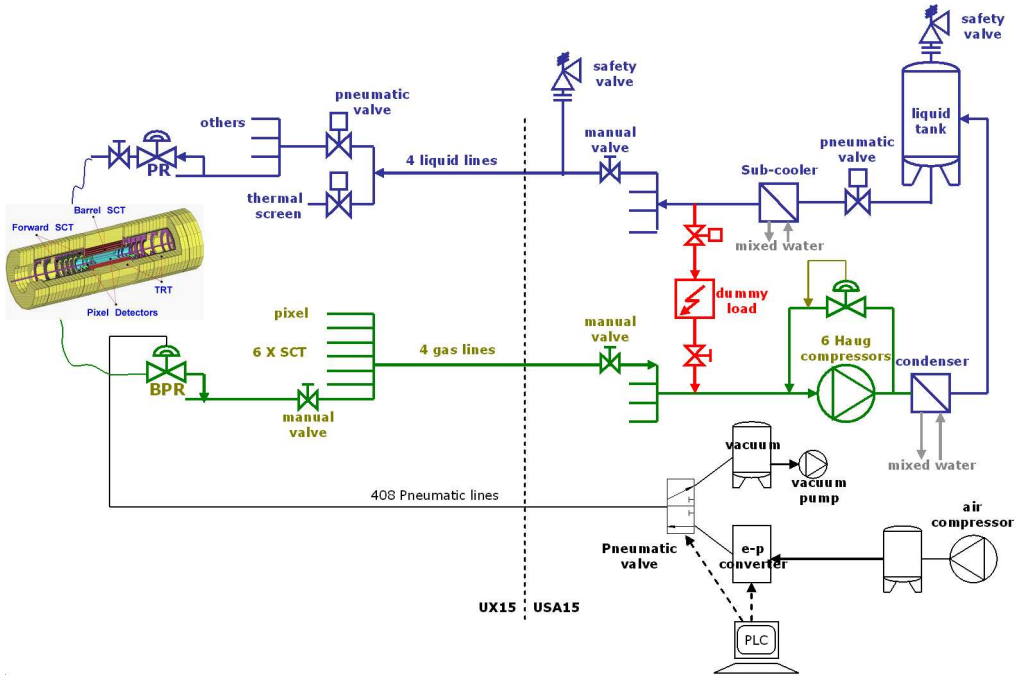

Figure 5. Schematic of the evaporative system main plant.

The liquid is than collected in a storage tank and is ready to be delivered again to the main inlet distribution manifold.

2008 JINST 3 P07003

Figure 6. Evaporative system main plant in USA15. Four compressors are visible (white housing).

The control of the main plant is based on a standard PLC.[5]

The compressor equipped with the by-pass line together with all other fundamental components to run the system (including the PLC, vacuum pump and back-up chiller for cold water supply to the heat exchanger) are powered by an Uninterruptible Power Supply (UPS) to guarantee a minimal operation in case of main power failure and to allow a safe fluid recovery from the detector.

4. System control

Each on-detector circuit of the evaporative system has a fixed expansion device, a capillary, thus fixed impedance. Therefore the pressure in the inlet tubes is a fixed function of the mass flow. This choice is driven by the need to minimizing the number of control devices in the detector volume given the extremely complicated access in case of maintenance. In fact the first fluid control devices, the pressure regulators, are located outside the volume of the experiment, 20 meters away from the ID.

It is critical to keep the fluid in the inlet lines up to the capillary in liquid state, therefore the inlet fluid pressure must be always above the saturation point, otherwise possible vapour formation will lead to a significant reduction of the mass flow through the capillary and to a significantly reduced cooling capacity.

The key problem is due to the variable heat load of each circuit which may vary over the full range 0%–100%. Each circuit is in particular requested to be started in stand-by mode with no load on it and to be able to cope with any power rump-up and rump-down transients.

[5]SCHNEIDER, model TSX-Premium

2008 JINST 3 P07003

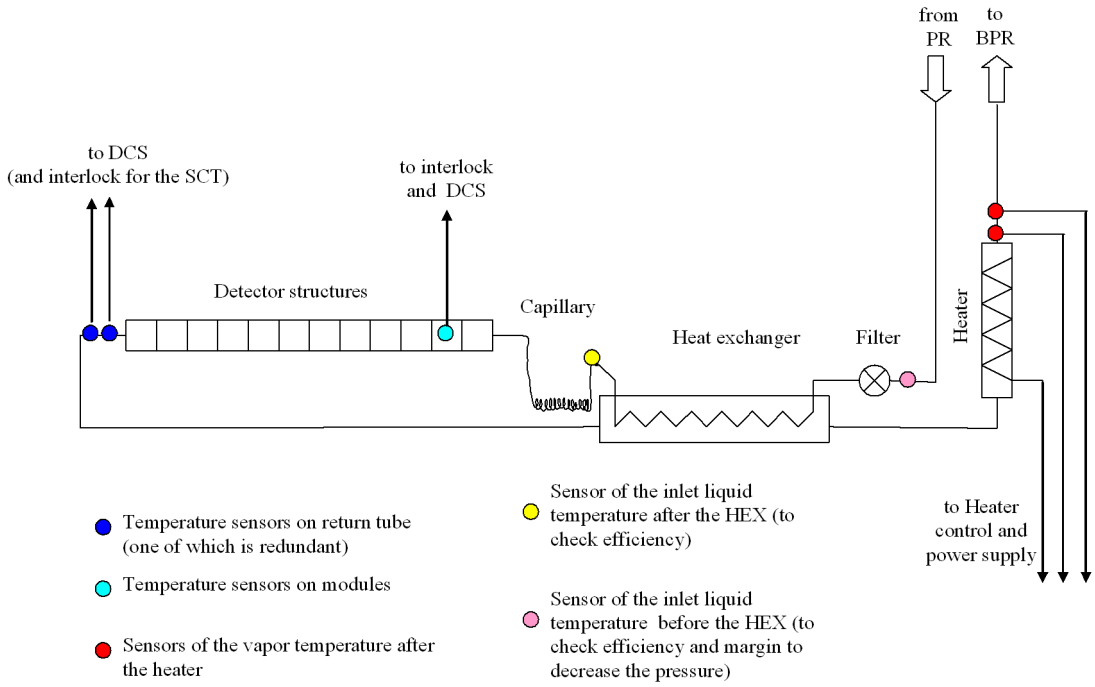

Figure 7. Schematic of the on-detector part of one circuit. The position of the various temperature sensors is shown.

Two opposite basic control strategies of the system were evaluated: varied flow and constant flow. A constant flow system was finally adopted.

With the constant flow approach each circuit is operated with a constant flow in on-off mode. When a circuit is set to “on”, the corresponding pressure regulator in the distribution rack opens and regulates the pressure in the inlet line at a constant value, allowing the fluid in the inlet lines to be always above the saturation point at room temperature. The flow can however be manually adjusted within a small range by changing the set point of the pressure regulator. A heater at the exhaust of each detector structure circuit evaporates the residual liquid and rises the temperature above the cavern dew point to avoid condensation outside the dry ID volume (figure 7).

The choice of the fixed flow system as against the varied flow option was driven by a number of arguments mainly related to the system integration in the context of the ATLAS experiment and to the system control strategy.

A varied flow system would have required an active cooling of the inlet liquid lines all the way down to the inlet of the capillaries in order to keep the inlet fluid temperature below the saturation temperature over the full range of mass flow, nominally from 0 to 100%. This translates into the requirement for the active system of being capable of maintaining the minimum temperature of the fluid in the inlet lines to preferably below -25 °C all the way in from the distribution racks to the detector. Given the tight space, especially around the ID volume and inside it, some length of the inlet tube bundles would have required an active insulation, i.e. a layer of insulation with an active heating foil around it to keep the temperature over the external surface above the dew point. In the fixed flow system the pressure in the inlet lines is constant during operation regardless the

2008 JINST 3 P07003

power load on the detector and has been chosen to be above the saturation up to a maximum design temperature of 40 °C. The inlet liquid it therefore warm all the way down to the inside of the ID dry volume and so in principle no insulation is required. However just some passive insulation was added around the inlet tubes in order to minimize heat pickup and hence the fluid temperature increase in the detector regions crossed by the inlet tubes where the ambient temperature might be significantly above the average cavern temperature. Therefore the insulation was added just to improve the system efficiency which, as shown later, is a function of the inlet temperature to the heat exchanger.

A varied flow control system was initially studied. This was based on a PID control algorithm receiving as feed-back the temperature read at the exhaust of the on-detector structures and varying the flow as function of the heat dissipation on the detector modules.

On the other hand a fixed flow system does not see changes of the operating parameters over most of the pipework except the area between the detector structures and the heater on the exhaust tubes. The active control is on a component, the heater, located at the exhaust of the detector circuit, not affecting the fluid conditions in the detector itself and having a small impact on the overall circuit, which remains in steady state conditions.

This approach was considered to be the less risky and hence adopted, though the varied flow option was proven to work on a prototype of part of the system implemented on a full scale mockup [13].

Compared to the varied flow system, the efficiency of the fixed flow system is lower in stand-by conditions when there is no load on the detector, which nevertheless should be only a fraction of the operation time. During operation at full load the system efficiency becomes closer to that of the varied flow system.

The heater power is controlled, by a PLC based PID system, in such a way as to maintain a temperature at the exhaust always around 20 °C: the changes in power load on the detector are compensated by changing the power supplied by the heater. Thus the total power supplied to each cooling circuit remains constant regardless of the power load on the detectors.

4.1 System operational modes

The system has several modes to enable safe operation of the plant and the detectors. These are detailed here:

- The plant is turned on and the plant is set to stand-by. The fluid is circulated internally in USA15 via a water cooled heat exchanger. The fluid does not go to the racks.
- The system is in the stand-by mode. The fluid is sent to the racks but the PRs are closed so no fluid flows to the ID.
- The system is in run mode. The PRs and BPRs are open, the return heater system is on and regulated by the PLC. The fluid circulates inside the ID and cools the detector.

There are two default run modes, the cold and the warm operation modes. The cold operation is required for the final operation of the experiment and the back pressure is set to obtain an evaporation temperature of -25 °C. The warm mode is sub-detector dependent and has an evaporation

2008 JINST 3 P07003

temperature that allows safe commissioning of the sub-detector while the dry environment cannot be guaranteed. For the SCT barrel this is 6 bar absolute or 6 °C. For the SCT end-cap the evaporation temperature will have to be close to 0 °C due to the resistances in the end-cap thermal path from module to cooling fluid. The Pixel disks cannot run warm as the structure can not withstand high pressures and therefore blow-off valves have been added to the Pixel disk vapour return lines to protect them.

5. The on-detector part of the system

5.1 On-detector circuitry: layout and heat loads

The detector structures of the Pixel, SCT barrel, SCT end-caps are grouped in 204 independent cooling circuits. Each cooling circuit (figure 8) consists of one recuperative heat exchanger, 1, 2 or 3 capillaries, on-detector cooling loops, one heater at the exhaust of the detector structures and pipe work connecting all the components to the distribution racks via one pressure and one back pressure regulator.

2 and 3 capillaries are used on the circuits having 2 or 3 branches connected in parallel on the same inlet and return tube. Each parallel branch must be equipped with an independent capillary in order to set the correct mass flow in it.

Several temperature sensors are placed along the circuit to measure the temperature at the critical points. Some of these sensors are used as an interlock of the power supplies in case of temperature runaway, two of the sensors are used as feed-back for the control system of the heater on the exhaust tube and all the remaining sensors are just used for monitoring.

All the components shown in figure 8, which include all the cold parts of the cooling circuits, are inside the ID volume which is kept dry during operation by flushing dry N_2 and CO_2 in the detectors volumes and in the gaps between them.

Figure 9 shows the location of the heaters and heat exchanges in the ID volume:

- The cooling circuit of the detector structures and the capillaries are located inside the pixel and SCT gas enclosure
- The heaters are all located outside the Pixel and SCT gas enclosures
- The heat exchangers of the SCT are located in the gaps outside the SCT gas enclosure, while the heat exchangers of the pixel are located inside the pixel gas enclosure.

The required mass flow depends on the power dissipation of a specific detector structure, on the efficiency of the heat exchanger and on the vapour quality (VQ) at the exhaust of the cooling structures. The required mass flow is then typical for each circuit and it is set for each circuit by changing the geometry (length and ID) of the capillary. The length of the capillaries is tuned to give the right flow during the manufacturing process as the capillary length cannot be changed after the detector installation.

The tuning process of the capillary length is necessary to compensate for the slight changes of their diameter: given the fact that the mass flow varies with about the 4^{th} power of the diameter, even very small changes of the diameter could give significant changes in the mass flow.

2008 JINST 3 P07003

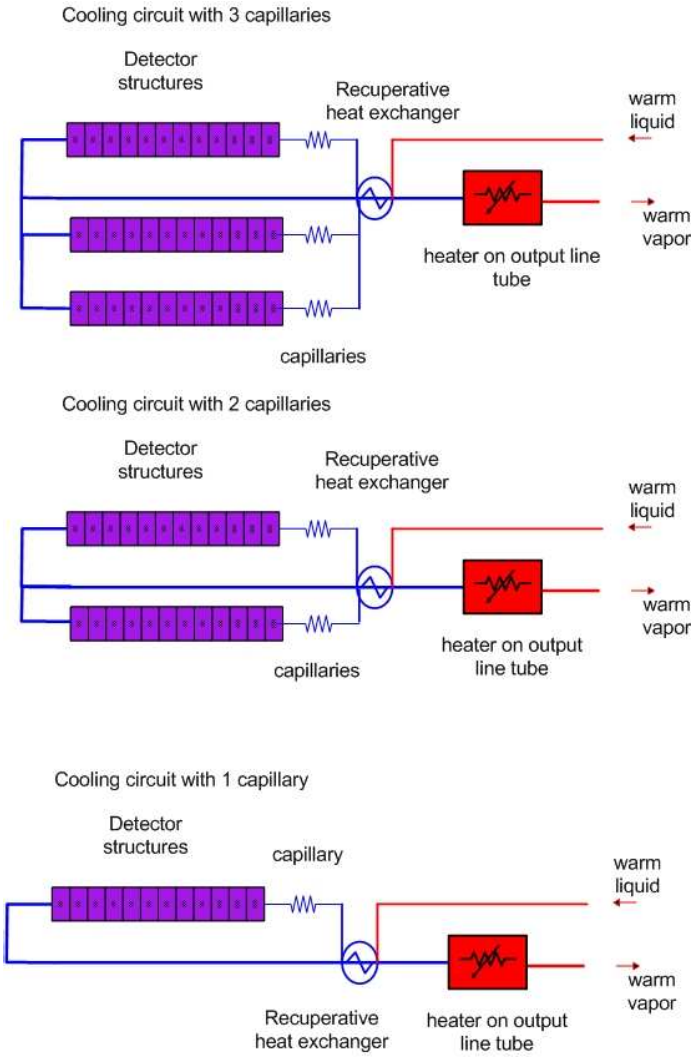

Figure 8. Configurations of the on-detector cooling circuits.

The aim of the length tuning process was to narrow-down the tolerance range of the nominal mass flow. This is important because the maximum flow drives the heater design power and also the pressure drop across the return tubes and both parameters need to be minimized.

The most critical parameter to be mastered in order to determine the minimum flow is the efficiency of the heat exchanger. The heat exchanger efficiency is a function of the fluid mass flow, of the fluid speed, of the liquid fraction at the inlet and it also depends on the heat exchanger orientation. Moreover higher fluid speeds also imply higher pressure drops, which is not desirable. A long test plan on prototypes has been carried out in order to optimize the design of the heat exchanger finding the best compromise between all the parameters leading to the minimization of the nominal flow. Table 3 gives the nominal heat loads and the nominal mass flow for the various circuits of the ID evaporative system.

2008 JINST 3 P07003

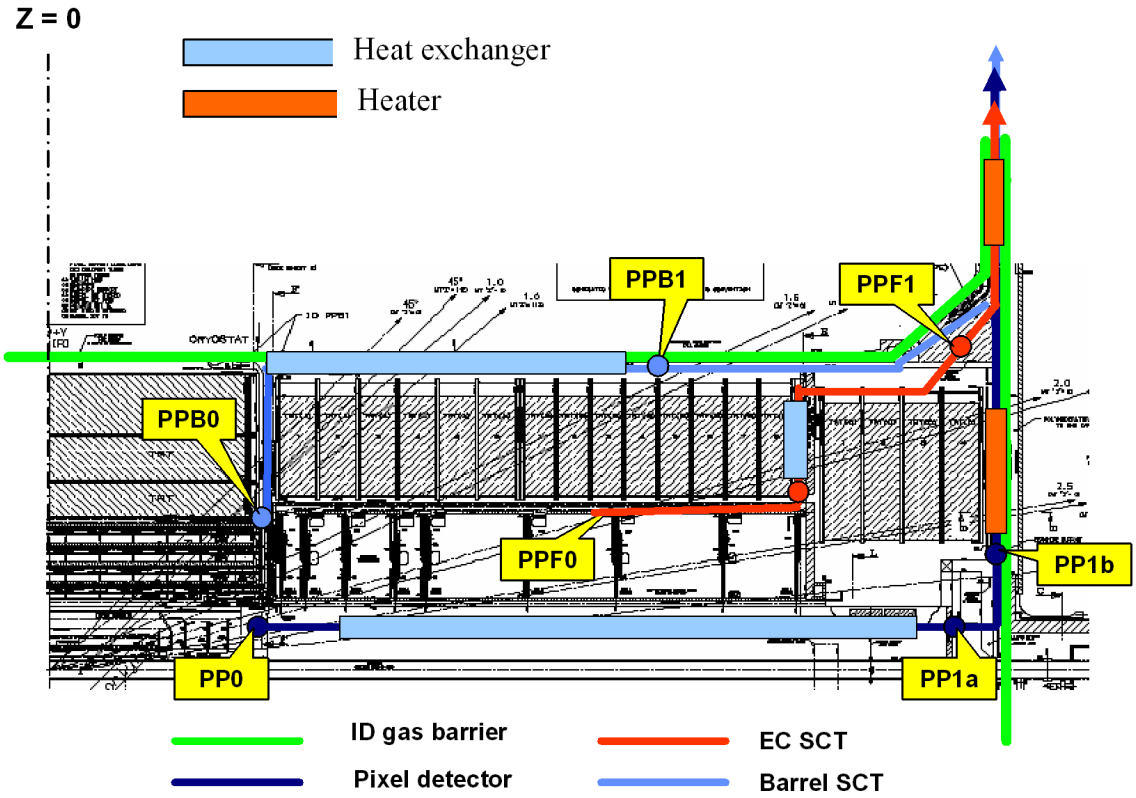

Figure 9. Location of heaters and heat exchangers inside the ID volume. PP__ indicates a break point.

Table 3. The basic parameters and cooling capacity of the internal evaporative circuits.

	Numbers of capillaries per circuit	**Number of circuits**	**Nominal power load per circuit**	**Subtotal nominal power load**	**Nominal mass flow per circuit**
			[W]	[kW]	[g/s]
SCT Barrel	2	44	504	22.2	7.8
SCT EC (3 sectors disk)	3	64	346.5	22.2	5.7
SCT EC (2 sectors disk)	2	8	241.5	1.9	4.5
Pixel Barrel	1	56	220	12.4	4.1
Pixel Discs	1	24	110	2.7	2.1
Pixel service panels	1	8	220	1.8	4.1
TOTAL		**204**		**63.2**	

5.2 The ID evaporative test station

A test station (figure 10) of the evaporative system was built to test and qualify all the components of the system (capillaries, heater, heat exchangers and on-detector module cooling structures).

2008 JINST 3 P07003

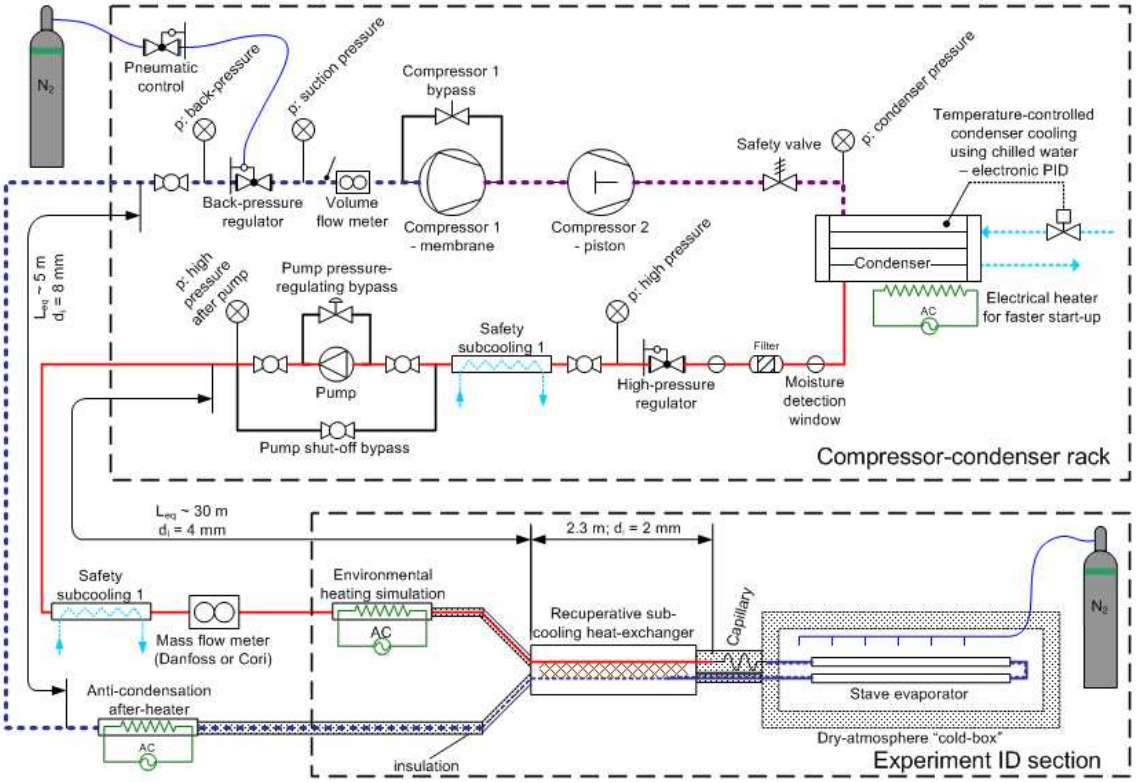

Figure 10. The test station of the evaporative system.

The test station was able to reproduce at the inlet and outlet of each test component the same conditions of the final system and moreover it had the flexibility to adjust the input-output parameters over the operating range of the final system, thus allowing the exploration of the full parameter space.

5.3 Capillaries

5.3.1 Capillary design issues

The mass flow of C_3F_8 through the cooling pipes of the SCT and Pixel systems of the ID sub-detector are controlled by the capillaries in the circuit which are the circuits' expansion devices. The cooling system requires two identical capillaries for each SCT barrel stave, which consists of two cooling loops connected together at the vapour side. There is one capillary per cooling loop per disk quadrant for an SCT end-cap. The typical quadrant has three cooling loops, an outer, middle and inner cooling loop. Due to the different number of modules per loop (outer = 52; middle = 40; inner = 40) the heat load per loop differs and therefore so does the required coolant mass flow. For simplicity two capillaries were chosen; one for the cooling loops for the inner and middle modules and one for the outer cooling loop with a higher mass flow. The low mass power tapes for the end-cap were also actively cooled with four capillaries per quadrant supplied by the unused capillaries from disks 7, 8 and 9. The Pixel sub-detector has the requirement for four mass flows, two for the Pixel barrels and two for the Pixel disks and opto-packages, two types of capillary were

2008 JINST 3 P07003

required for each Pixel sub-detector as a consequence of a repair that reduced the inner diameter and thermal performance of a sub-set of detector cooling structures. There were therefore four unique capillaries for the Pixel system. In total 7 different capillaries were used.

The mass flow through a capillary increases with capillary inner diameter, and falls with the capillary length. The flow also increases with pressure drop over the capillary and falls with increasing liquid temperature before the capillary. The exact dependence of mass flow upon these quantities in case of a 2-phase flow is very difficult to calculate, given also the fact that the flow is sensitive to the exact physical nature of the capillaries. Therefore an empirical approach has been followed to precisely characterize the capillaries. The ID cooling system fixes the liquid drive pressure at the rack via a pressure regulator and fixes the vapour pressure at the rack using a back pressure regulator. Therefore the pressure drop over the capillary is fixed externally. As the pressure drop along the capillary is not linear with capillary length, measurements of mass flow were performed over a range of capillary lengths which covered those expected to be used in the final experiment. The limits on the capillary length were defined by the geometry of the sub-detector with the requirement that the capillary is sufficiently long to reach the cooling loop for the inlet line of the heat exchanger but not too long to be a problem to store inside the thermal enclosure.

The capillaries used for both the pixel and the SCT detectors were all annealed copper nickel (Cu/Ni30Mn1Fe) extruded tubes with a wall thickness of 0.2 mm.

Characterisation measurements were performed using four different inner diameters, which were nominally 0.65, 0.75, 0.9 and 1 mm. The inner diameters were measured very accurately by means of a liquid filling method.

The mass flow as a function of length, inlet fluid temperature and pressure drop over the capillary were measured for C_3F_8 around the final experimental operational point for each capillary inner diameter. From these measurements the required production capillary diameter and length were determined once the efficiency of the recuperative heat exchanger was known.

5.3.2 Characterization of the capillaries

The measurement of the flow through the capillary utilized the C_3F_8 compressor condenser evaporative test station described above. The C_3F_8 liquid under high pressure from the test station was split into two streams each with an independent pressure regulator with a delivered maximum pressure of 16 bar absolute. The first went via a liquid Coriolis effect based mass flow meter through a heat exchanger to a manifold; to which the capillaries under test were attached. This enabled the mass flow through a given capillary to be measured. The second stream went via a capillary to the cooling circuit of a heat exchanger on the liquid line before the capillary under test, which was used to control the temperature of the liquid before the test capillaries. To test the capillaries at an elevated liquid temperature (up to 40 °C) a kapton heater was attached to the liquid inlet pipe between the heat exchanger and the capillaries under test. The liquid's temperature and pressure were monitored just before the test capillaries and immediately after them.

Capillaries with four different nominal ID values were tested: 0.65, 0.75, 0.9 and 1 mm. Capillaries of length 1.5, 2, 2.5, 3, 4, 5, and 6 m were cut for each ID value. A given capillary was switched into the circuit and measured independently. The temperature and pressure of the coolant liquid before the capillary was set and the mass flow through and the pressure drop across the capillary was measured once stable flow conditions were obtained. The capillaries were tested

2008 JINST 3 P07003

Table 4. Test matrix of capillaries.

Lengths [m]	1.5, 2, 2,5, 3, 4, 5, 6
Nominal ID [mm]	0.65, 0.75, 0.9, 1.00
Input Pressure [bar abs]	10 to 16
Pressure Drop [bar]	8.25 to 14.25
Liquid Temperature [°C]	−15 to 40

under a range of pressure drops, defined by the input pressure as the evaporation pressure was fixed, and input liquid temperature. Table 4 gives the detailed test matrix of the capillaries.

From the measurements of mass flow, the mass flow was plotted as a function of each of the variables and fitted with a polynomial so that the results could be used as a predictive tool for the required capillary inner diameter when the boundary conditions of a reasonable capillary length, a fixed input liquid pressure (fixed at 13 bar absolute to maintain the liquid above the saturation temperature at all times), a measured liquid temperature and a required mass flow from the heat exchanger measurements were known. Figure 11 illustrates the pressure drop over the capillary as function of the mass flow of C_3F_8 through it, for capillaries with ID of 0.65 mm for 5 different capillary lengths and with a liquid temperature before the capillaries of 20 °C. As expected the mass flow is a linear function of pressure drop. As can be seen the gradient of mass flow as a function of pressure drop changes by about 40% with capillary length over the measured values.

Figure 12 shows the mass flow through a capillary as a function of capillary length, for the four capillary IDs tested; a liquid temperature before the capillary of −10 °C and a pressure before the capillary of 13 bar absolute, which corresponds to a pressure drop of 11.25 bar were used.

Figure 13 shows the mass flow through the capillary, as a function of capillary inner diameter, ID, for capillaries of lengths between 1.5 m and 4 m, with a liquid temperature before the capillary of −10 °C and pressure drop of 11.25 bar.

Finally the mass flow as a function of liquid temperature before the capillary is illustrated in figure 14 for a capillary of ID of 0.65 mm, length of 2 m, and evaporation pressure of 1.75 bar absolute for 4 input pressures. The change in mass flow over the capillary, for a change in liquid temperature before the capillary from −15 °C to 20 °C, for an input pressure of 13 bar absolute, was 0.42 g/s or 24%. As can be seen in figure 14, for the data measured with an input pressure of 14.5 bar absolute, for temperatures above 20 °C the mass flow is less than that predicted from the simple linear fit.

There is no reason to assume a priori that the behaviour will be linear and the fits, performed on the limited data set, are valid only over a small change in temperature. For example, with an input liquid pressure of 14.5 bar absolute, which corresponds to a saturation temperature of 45 °C, and an input liquid temperature of 40 °C the mass flow is overestimated from the simple linear fit to the data obtained between −15 °C to 20 °C by 0.33 g/s or 33%. The fall in the mass flow as a function of increasing input liquid temperature implied that the temperature of the fluid before the capillary had to be maintained at a relatively constant value. This was achieved with the use of the recuperative heat exchanger in the circuit and the positioning of the capillary after the heat exchanger rather than inside it.

2008 JINST 3 P07003

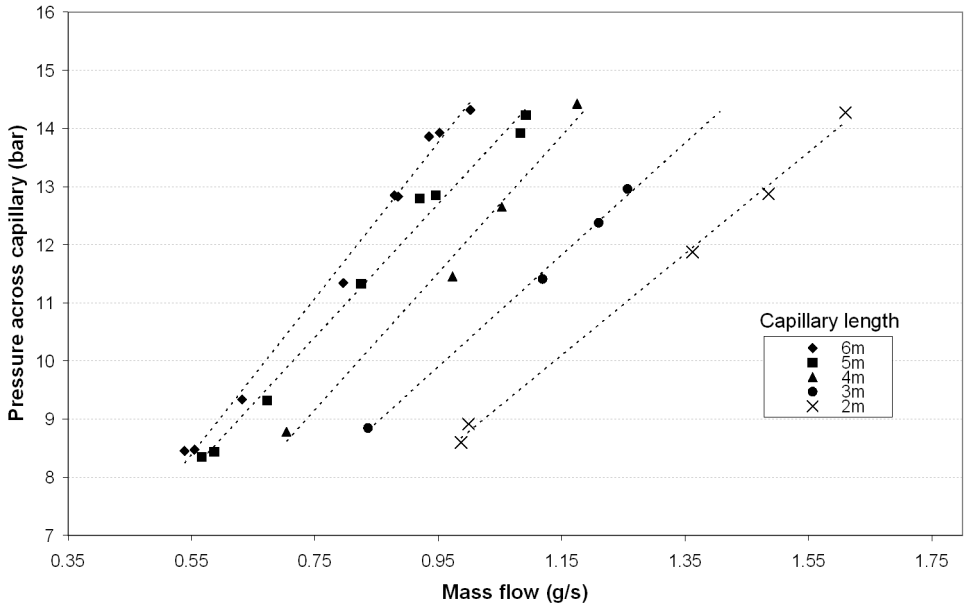

Figure 11. Pressure drop across against mass flow through capillaries with a nominal ID of 0.65 mm with a liquid temperature before the capillary of 20 °C and an evaporation pressure of 1.75 bar absolute, for 5 different lengths defined on the graph.

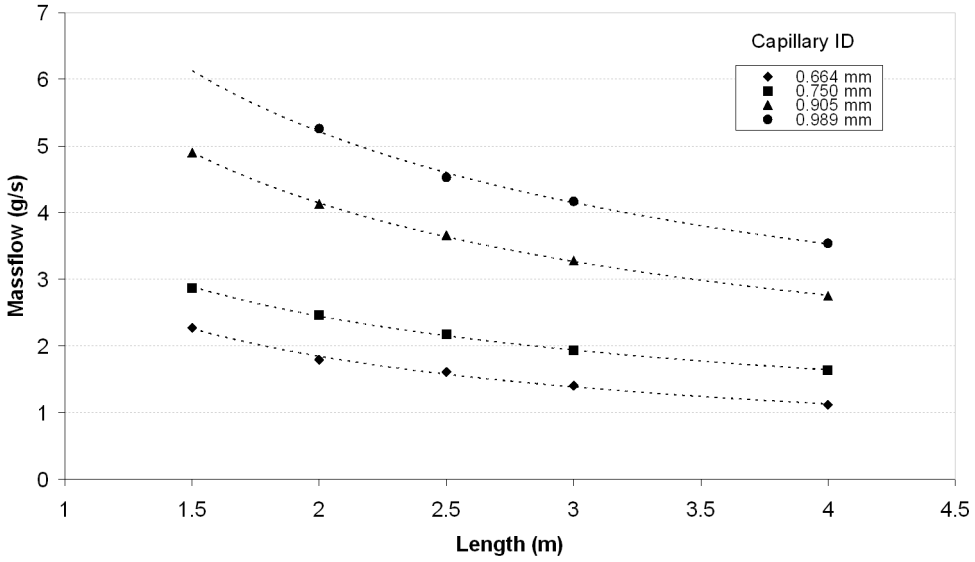

Figure 12. Mass flow as a function of capillary length, for a liquid temperature before the capillary of −10 °C, a pressure drop of 11.25 bar and an evaporation pressure of 1.75 bar absolute, for 4 values of ID defined on the graph.

5.3.3 Capillary choice and tuning

From the fits to the plots of figure 11 to figure 14, and similar plots, the dimensions of the required

2008 JINST 3 P07003

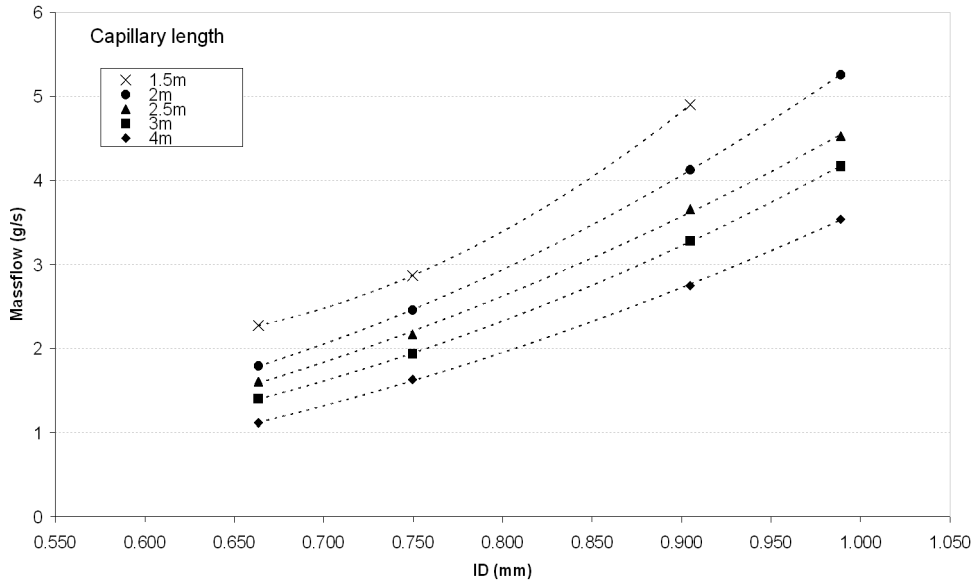

Figure 13. Mass flow as a function of capillary ID; measured for a liquid temperature before the capillary of $-10°$C, a pressure drop of 11.25 bar absolute and an evaporation pressure of 1.75 bar absolute, measured for 5 different capillary lengths, noted on the graph.

capillaries for the evaporative cooling system were predicted. The pressure of the liquid before the capillaries was know and fixed at 13 bar absolute, while the evaporation pressure was fixed at 1.75 bar absolute, which corresponded to a nominal pressure drop over the capillaries of 11.25 bar. The temperature of the liquid before the capillaries was not known at the time of the order of the capillary, as the full tests of the recuperative heat exchangers had not been performed, but was estimated to be -10 °C based on previous experience.

Even a small change in ID of +/-20 μm, which is a typical tolerance range of the manufacturers, produces a change in the mass flow of the order of +/-7%. Therefore, in order to reduce as much as possible the expected mass flow variations due to the manufacturing tolerances of the capillaries, it was decided to individually tune all of them.

From the experimental data an estimation of the variation in the required length of the capillary to compensate for a change in the capillary ID was made. A change in length of +/-15% of a typical capillary produces a change in mass flow of the order of +/-7%, thus compensating the expected change in ID of +/-20 μm. The nominal capillary length was then chosen to be sufficient at the maximum expected negative length compensation. Once chosen, the nominal length, the ID of the capillaries was finally determined. Table 5 lists the nominal capillary parameters: mass flow and corresponding length and ID.

A production station was set-up to perform the tuning of all the capillaries. The station measured the mass flow of C_7F_{16} in mono-phase conditions through a capillary for a given input pressure and temperature which was compared to that given by a reference capillary. The capillary length was then cut to increase the flow as required until the flow was equal to the reference capillary with an accuracy of +0% / -2%.

2008 JINST 3 P07003

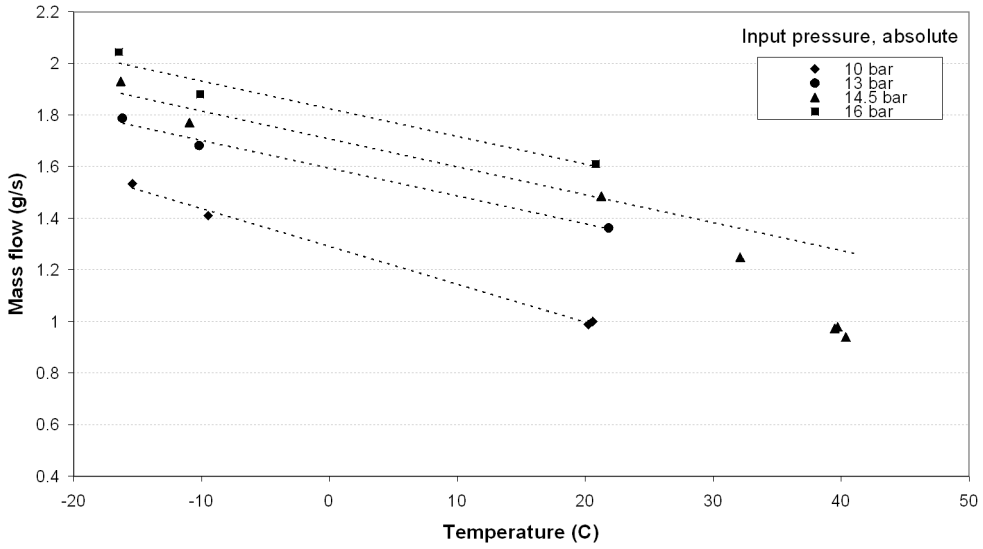

Figure 14. Mass flow as a function of liquid temperature before a capillary, measured for capillary with a nominal ID = 0.65 mm, and length of 2 m, with an evaporation pressure of 1.75 bar absolute with different input liquid pressures which are defined on the graph. The linear fits shown are performed for temperatures from 20 °C to −15 °C and are to guide the eye and illustrate the non-linear dependence of the massflow on liquid temperature.

Table 5. The capillary nominal design parameters.

CIRCUIT	MASS FLOW (g/s)	ID (mm)	Length (mm)
Barrel SCT	3.9	0.75	500
EC SCT (inner and mid sector)	1.6	0.75	2500
EC SCT (outer sector)	2.1	0.68	2500
Pixel barrel and opto-boards	4.1	0.8	1200(*)
Pixel discs	2.1	0.55	1250

(*) 1100 mm for the circuits having one stave with increased thermal impedance (“inserted” stave).

A different approach was used for the pixel capillaries due to the limited time and resources. A simulation model [14] of the capillary flow was used to predict the initial geometry and speedup the process. As for the SCT capillaries, the test station in figure 10 was then used for the final capillary length adjustment and to produce the reference capillary. All needed capillaries were then produced by trimming them against the reference capillaries at the test station using the nitrogen flow analogy.

5.4 Heat exchangers

5.4.1 Heat exchanger design

The design of the heat exchanger (HEX) was sub-detector dependent, while the detailed design of

2008 JINST 3 P07003

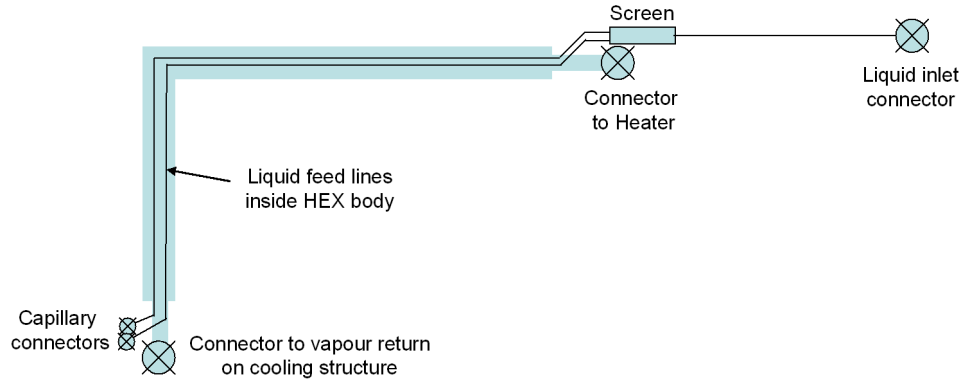

Figure 15. Schematic of the SCT barrel HEX showing the two inlet pipes inside the vapour return tube.

the HEX varied depending on the detailed routing required for the HEX; typically each HEX in a given quadrant is unique. All are simple and low mass in design. The HEXs were counter flow devices using the returning fluid from the detector cooling structure to cool the incoming liquid.

The SCT HEXs are constructed from thin walled Cu and CuNi pipes with CuNi connectors, while the Pixel HEXs are made in aluminium.

At the start of the HEX the inlet pipe incorporated a screen filter to prevent the passage of small items into the capillaries, which could cause a blockage. The screen consisted of 264 0.5 mm diameter holes. The screen is not accessible after installation and therefore prior to installation the removal of particulates from the off-detector system was performed.

After the screen the inlet pipe entered the HEX, for the barrel HEX this was via a peek based electrical break to electrically isolate the detector structures from the rest of the ATLAS experiment.

The capillary, or capillaries, were connected to the inlet line after the HEX, the other end of which was connected to the sub-detector's cooling circuit. The return fluid from the detector cooling circuit passed via a manifold and some length of pipe work to the vapour side of the HEX. For the barrel HEX the peek based electrical isolation on the vapour side was mounted in the fluid connector between the HEX and the vapour return heater. For the SCT end-cap HEX the peek based electrical isolation was mounted on the detector side of the HEX for both inlet and vapour return lines.

Schematics of the SCT barrel, SCT end-cap and Pixel HEXs are shown in figure 15 to figure 17. The Pixel design differed from those of the SCT in that the inlet liquid pipe was simply glued to the outside of the return vapour line, while for the SCT HEXs the inlet pipe was placed inside the vapour line.

Due to space constraints the length of the end-cap HEX (37 cm) was significantly shorter than the barrel HEX (150 cm) and therefore the inlet pipe had to be coiled inside the end-cap HEX to increase its contact surface area with the return fluid in order to obtain sufficient efficiency.

The Pixel design was possible as the HEX length was sufficient (1.5 m) to give the required heat transfer efficiency. The increased efficiency of the immersed inlet pipe had the negative consequence of increasing the pressure drop on the vapour return line due to the reduced free cross-sectional area of the return pipe. The external diameter of the vapour return pipe being limited due to space limitations inside the tracker, the barrel HEX had an external vapour return pipe diameter of 15 mm while the end-cap was only 14.4 mm.

2008 JINST 3 P07003

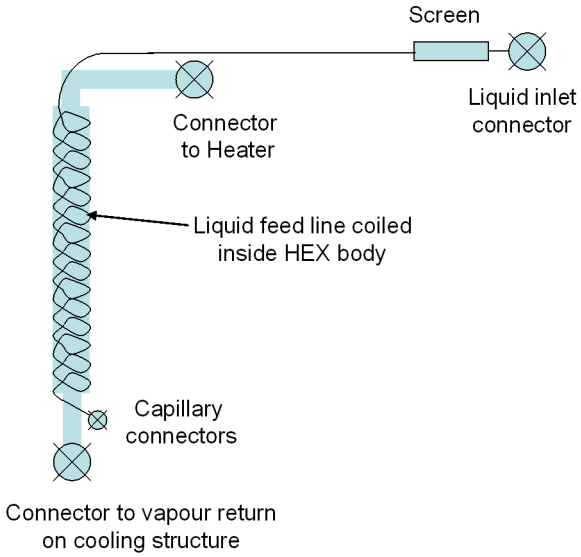

Figure 16. Schematic of the SCT End-cap HEX showing the coiled inlet pipe inside the vapour return tube.

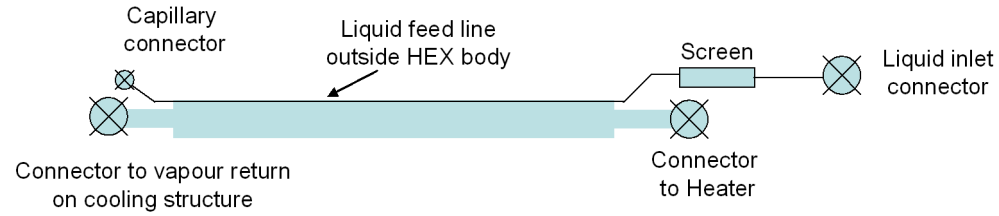

Figure 17. Schematic of the Pixel HEX, showing the liquid inlet pipe glued to the outside of the vapour return tube.

5.4.2 Heat exchanger tests

The efficiency of the HEX, η, can be defined according to equation (5.1),

$$\eta = \frac{T_0 - T_1}{T_0 - T_2} \tag{5.1}$$

where T_0 is the inlet liquid temperature, conservatively assumed to be 35 °C, T_1 is the sub-cooled liquid temperature after the HEX, and T_2 is the evaporation temperature in the structures, designed to equal −25 °C. The higher the efficiency of the HEX the lower the input temperature to the capillary, the lower the input vapour quality to the detector structures, and therefore the higher the cooling capacity of the system for a given mass flow.

The details of the design of each sub-detector cooling system were prototyped outside of the ATLAS experiment on a complete cooling circuit per sub-detector with the ID evaporative test station. The system was shown to be able to remove the detector's heat load for an inlet liquid with a temperature as high as 35 °C, a conservative upper limit, for a mass flow that was minimal as given in table V, with an expected pressure drop close to or below the maximum permissible on both the liquid (1000 mbar) and vapour (350 mbar) lines. The system was shown to be stable for a long duration of operation at the nominal conditions, with one run performed continuously for 90

2008 JINST 3 P07003

hours. The system was shown to be able to function correctly in response to sudden changes in the power load of the detector from zero to full power. The detector power was switched from 0% to 100% of nominal power as fast as possible by flicking the main switch to the bench power supplies supplying the heat load to the circuit. This is expected to be as fast as or faster than the power transients in the final system. The system returned to stability after approximately 20 minutes to such a change in power, where stability was defined as constant and operable temperatures in the system. The cooling loop was run at 100% for over 2 hours to show that the system was stable, after which the power was switch back to 0%. This cycle was repeated several times to demonstrate repeatability. If the system operated correctly stability was always achieved after each switch in detector power.

The SCT end-cap HEX is positioned in the experiment at a slope of 45 degrees above and below the horizontal, with the HEXs in the upper quadrants of the end-cap having their vapour inlets from the detector at their lowest point, that is they point upwards; while the HEXs serving the lower 2 quadrants have their vapour inlets at their highest point. It was observed that the efficiency of the end-cap HEX was dependent upon this orientation. The HEXs that point upwards demonstrated the highest cooling efficiency (approximately 85% with the inlet liquid sub-cooled to -13 °C) for nominal operating conditions compared to the downward orientation (only 70% efficiency and an inlet liquid cooled to -6 °C). However the measured mass flow was only marginally affected increasing by only 1.5%. The SCT barrel HEX has a similar geometrical layout in the experiment except that there is always a long horizontal section to the HEX as well as a radial component. For this reason no measurable difference in performance was observed as a function of orientation for the barrel HEX. The Pixel HEX is installed, and therefore only tested, in the horizontal plane.

The mass flow increased for reduced inlet liquid temperature or detector power load, due to an increase in the efficiency of the HEX, which results from a reduction in the lower vapour quality at the inlet of the HEX. The mass flow increase was shown to be approximately 7% for the barrel system and by 9% for the End-cap system when the detector power was turned off and the inlet temperature was reduced to 20 °C.

The increased efficiency of the system associated with the lower inlet liquid temperature implies that a system is stable for higher detector power loads. For the SCT barrel the cooling system is stable with a detector power load equal to 140% of the nominal 504 W, which is 716 W. For the SCT End-cap the system is stable with 120% of the nominal power, that is 416 W.

A reduction in the mass flow for nominal detector power is possible if the incoming liquid is below 35 °C. This is achieved by reducing the pressure of the liquid feed line, while ensuring it remains above saturation conditions. It was shown that for an inlet liquid temperature of 20 °C and a reduced feed pressure of 11 bar absolute, well above the saturation pressure of 7.6 bar absolute at 20 °C, the mass flow fell by 10% for the end-cap HEX, while the efficiency only fell by 1% and the vapour quality of the fluid into the HEX increased from 0.66 to 0.72. The pressure drops over the liquid and vapour side of the HEX system were also reduced with reduced mass flow, as expected, because the effect of increased vapour quality at the detector output was outweighed by the reduction in mass flow.

Several quadrants (Disk 1) of the end-cap only have two cooling loops, (serving middle and outer modules), and therefore the HEX was studied with two capillaries and the full power reduced accordingly to 241.5 W. The HEX was found not to be stable with a mass flow reduced in proportion

2008 JINST 3 P07003

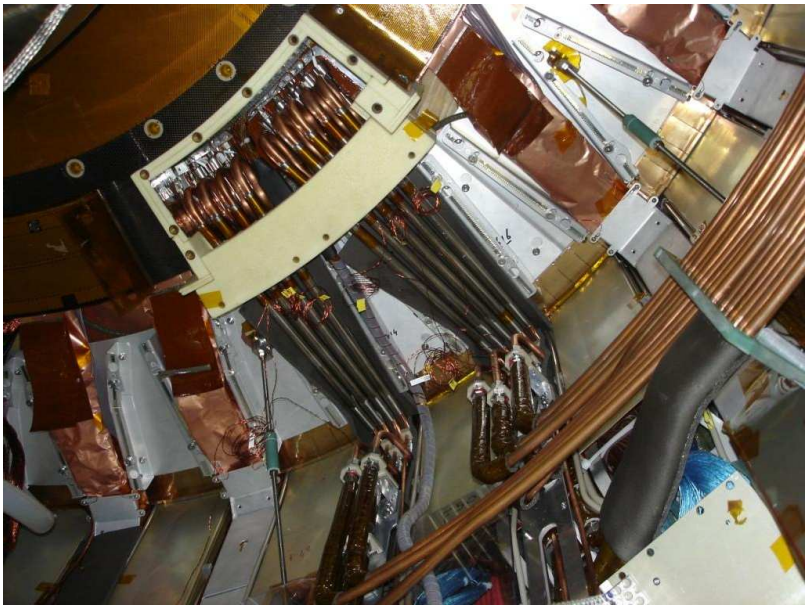

Figure 18. The SCT Endcap HEXs as installed in the inner detector.

to the power load; that is 3.98 g/s rather than 5.7 g/s. The minimum mass flow that allowed stable operation was 4.4 g/s, which corresponds to that obtained from two larger (0.75 mm) ID capillaries instead of a large and small ID capillary. The pressure drop over the middle on-disk cooling loop will increase due to the 24% increase in mass flow through this loop, while the mass flow through the outer cooling loop remains the same. This increase in pressure drop over the middle cooling loop will be negated by the lower pressure drops over the off-detector system as the total mass flow has fallen. Therefore the HEXs that served just two cooling loops use two larger ID capillaries.

As, typically, each inlet line feeds more than one capillary, (2 for the SCT barrel and 2 or 3 for the SCT end-cap), the system must also be robust to blockages in one capillary which would reduce the flow through the HEX and therefore reduce the efficiency of the heat exchanger. It was shown that for the SCT end-cap that the efficiency fell such that for a HEX with two operational capillaries (outer and middle loops) the power that could be removed in stable operation was only 90% of the nominal power of the two cooling loops. Increasing the input pressure to 14 bar absolute enabled the HEX to regain the lost efficiency and remove the full power of two loops. For the SCT barrel the power that could be removed fell to only 88% for the nominal power of one cooling loop, due to the reduced efficiency of the HEX. In this condition the vapour quality at the entrance to the HEX was the same for the two loop operation.

Figure 18 shows a photograph of the SCT Endcap HEXs as installed in the inner detector. The HEXs, grouped into two bundles, one of 4 and one of 5, serve one quarter of the total cooling circuits of a given Endcap; in this case the circuits in the bottom left quarter of each disk, as viewed looking out from the interaction point.

2008 JINST 3 P07003

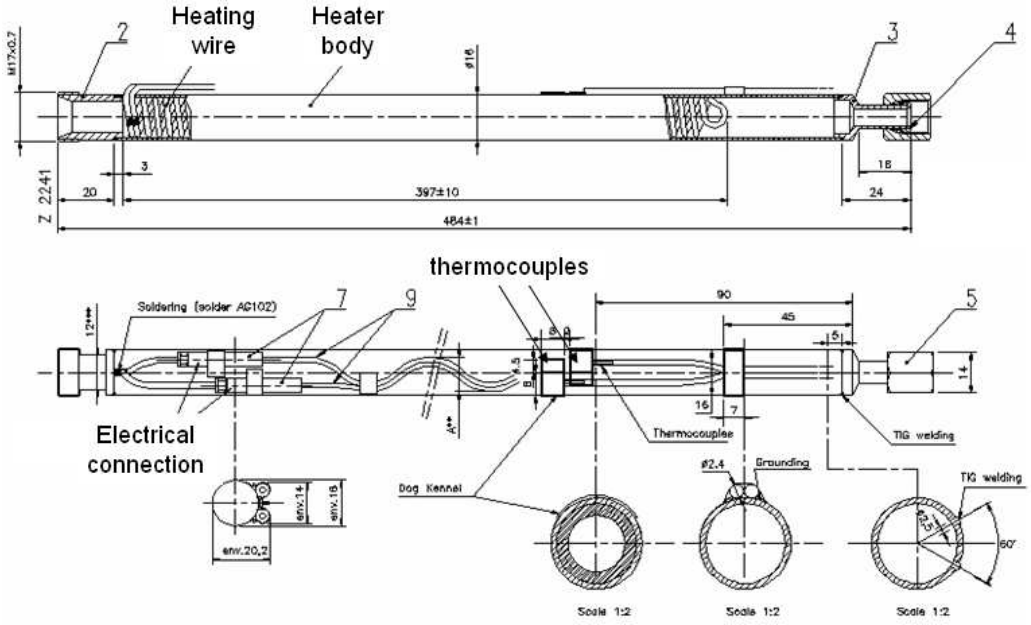

Figure 19. SCT barrel heater assembly drawing.

5.5 Heaters

5.5.1 Heater design

In order to minimize the space occupancy and to maximize the efficiency, the selected design of the heater at the exhaust of the detector structures consists of a coiled heating element placed inside a section of the return tube[6] (figure 19). The heating element is in contact with the tube walls. The heating length of the heating element, the diameter, the pitch and inner diameter of the coil have been selected in order not to exceed a maximum temperature of the heating element during operation of 100 °C (to have a sufficient safety margin against the decomposition of the fluid which starts to be significant at temperatures above 200 °C) and at the same time keep the pressure drops across the heater within a budget of 50 mbar. The final design parameters of the heaters are given in table 6. This type of heater is very efficient since the heating element is in direct contact with the fluid. This is demonstrated by the fact that for the circuit with the largest power, a heated length of the return tube of about 500 mm is enough to boil all the liquid when there is no power on the modules and to raise the temperature of the fluid at the exhaust up to 20 °C with a max temperature of the heating element of less than 80 °C.

The position of the heating element, internal to the tube, also minimizes the outer tube temperature, which, in the worst case, does not exceed 40 °C, thus also minimizing the required thickness of the insulation on the tube itself, which can be as small as 5 mm.

The heating element consists of a heating wire which runs along the axis of an outer metallic clad providing the required mechanical strength. The heating wire is fully embedded into a compressed electrical insulating powder (Magnesium oxide). The heating wire is made of a hot part and a cold part.

[6]THERMOCOAX custom design

2008 JINST 3 P07003

Table 6. Heater design parameters.

Circuit	Nominal power load on the detector	Heater design power	External tube inner/outer diameter	OD heating wire	Hot length	Coiled length	Coil pitch	Free diameter	Heat transfer area (1)	Specific heat flux (2)
	W	W	mm	mm	cm	mm	mm	mm	mm^2	W/cm^2
SCT Barrel	504	960	14/16	2	331	397	4.6	10	208	4.55
SCT EC	346.5	650	11/13	1.15	363	390	3.3	8.7	131	4.81
Pixel Barrel/opto-board	220	480	11/13	1	373	390	3.3	9	117	3.98
Pixel Discs	110	260	11/13	1.15	402	390	3.0	8.7	145	1.77

(1) External area of the heating wire over the hot length.

(2) Heater design power / heat transfer area.

The hot part is made of Constantan or Ni 80/20 and it is located completely inside the return tube. The cold part is made of copper and is located at both ends of the heating wire, where the heating element penetrates the tube wall and connects to flexible power cables through ceramic insulated special connectors. In the original design the electrical insulation was obtained using radiation hard epoxy resin, this solution was cheaper but did not survive long lifetime tests.

The penetrations of the tube are both located at the same place and so the internal heating element makes a double coil with a 180° turn at the far end.

The temperature feedback for the heater control system is provided by 2 thermocouples (one spare) located on the exhaust tube a few centimetres away from the heater end. Two thermocouples (one spare) are also fixed on the heater tube outer surface in the area reaching the maximum temperature; these thermocouples are connected to the interlock system of the heater control. The thermocouples are all of type E (Nickel-Chromium/Constantan).

5.5.2 Heater powering system and control

In order to minimize the injection of noise to the ID from the heaters during operation, DC power supplies have been employed.

From the point of view of the power supply cables it was preferable to use a high voltage as this minimizes size, occupancy and cost. Combining these constraints with safety requirements the heater system is powered with 0 V and -110 V voltages referenced to the overall ground.

This configuration of the supply voltage is still below the 120 V limit that defines the system as Functional Extra Low Voltage. Therefore standard precautions have been taken in order to provide the protection against direct contact. The protection level of the front side of the rack is IP30, the rear side of the rack with the distribution bars is secured by grounded grills and doors, and finally, all connectors are LEMO type with protection level IP50.

The maximum power requested by the heaters used by the evaporative cooling system is in the range of 126 kW. In addition to that, system must deliver additional short circuit current (>=100

2008 JINST 3 P07003

A) in case of faults, and must be capable to work in case of single failure in one of the rectifiers. Finally, the Distributed Power Supply (DPS) system is split into four racks, each one consists of thirty 1.5 kW rectifiers, capable to deliver up to 160 kW of redundant power to the heaters (typical efficiency of the converters is in the range of 91%). In order to minimize the length of the power cables, the DPS supply system is distributed on both sides of the experimental cavern. As can be seen in figure 20, half of the racks with the rectifiers are located in the USA15 and half in the US15 caverns. The location of the four, 64-channel Programmable Logic Controllers (PLC) used for controlling of the 204 heater elements is the USA15 service cavern.

For each heater (exhaust tube) there are two temperature sensors: one for the control function and a second for safety, to protect against over temperature of the heating element. The temperature signal is read out by an industrial PLC providing control of a MOS transistor switch turning ON and OFF the current supplied to the heater. The use of the MOS transistor as a switch device has been determined by the possibility of precise control of inrush current magnitude, and reduction of high frequency noise associated with high voltage and current transitions, since dv/dt and di/dt transitions are accurately controlled.[7] The driving circuit provides extension of the transition times up to about 3 ms, effectively limiting the frequencies of the radiated noise to values far away from the bandwidths of the sensitive front end electronics of the ATLAS detectors.

The safety sensor is read out by the interlock system which provides an interlock signal for each MOS switch.

The basic control loop and location of various components for the heaters of one cooling circuit are shown in figure 20.

Since the US15 cavern is not accessible during operation of the experiment, each DPS power supply rack can be remotely switched ON or OFF by a PLC controller located in the USA15 service cavern.

This feature is also used for the supplementary safety interlock, when the PLC receives fatal alarms from the monitoring (DCS; Detector Control System) or safety (DSS; Detector Safety System) systems. The integrated values of the current delivered to the heaters, the temperatures of the safety sensors as well as status of the interlocks and various alarms issued by the system components, are delivered to the ATLAS DCS system.

5.5.3 Heater system qualification

The qualification of the design of the heaters and of their powering and control system was performed on several prototypes tested in the ID evaporative test station.

The qualification procedure involved the measurement of the pressure drops across the heater, the maximum temperature of the heating element and the investigation of the stability of the control system against the various power loads and the worst case transient scenarios.

The tests led to the optimization of the position of the temperature sensor for the control allowing the measurement of the correct average temperature of the fluid at the heater exhaust and at the same time giving a sufficiently small response to ensure a stable operation (minimizing the temperature fluctuations). It was found that for the heaters of the SCT the control sensors could

[7] C.S. Mitter, Motorola SEMICONDUCTOR APPLICATION NOTE AN1542/D

2008 JINST 3 P07003

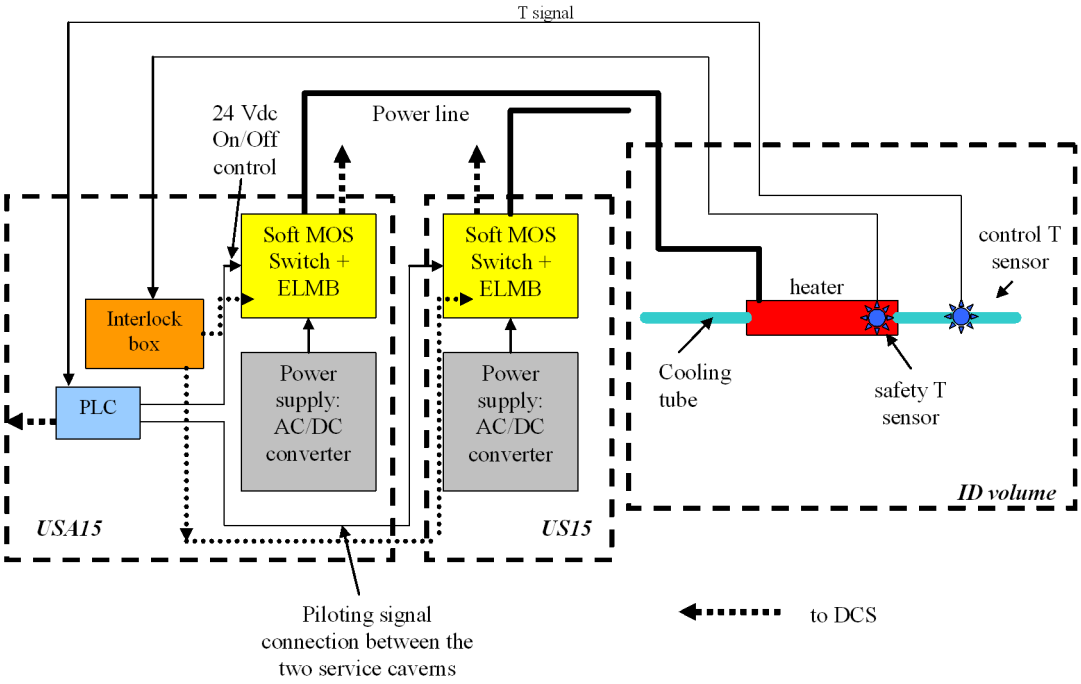

Figure 20. Schematic diagram of the heater powering and control system.

be placed on the outer wall of the exhaust tube, while for the Pixel heaters the sensors had to be immerged into the fluid stream to allow sufficient control stability.

The tests also led to the optimization of the position of the temperature sensor for the interlock system. In this case the location of the sensors on the heater outer surface at the end of the heating element coil was found to give a sufficiently fast response time to allow safe power interlocking with acceptable maximum temperatures of the fluid.

A typical heater transient from 0 to 100% power on the detector, which was tested during the qualification, is shown in figure 21.

The PLC control aims to keep the temperature measured from the control temperature sensor to be equal to a set-point temperature defined in the control software. In figure 21 the set-point is observed to change as the requested duty cycle suddenly falls due to the detector power load increasing from 0% to 100% of the nominal SCT barrel detector cooling loop power load. The PLC samples the temperatures of the heater at a rate of kHz and performs averages on the data to reduce the effective sampling rate to 100 s of Hz. The PLC acts upon the information at a rate of 2 Hz.

6. Pressure drops in the cooling system

6.1 Off-detector system

The pressure drops in the test system were measured for the individual items; heat exchanger, heater, on-detector cooling loops and for sections of pipe work. For these the total pressure drops in the cooling systems were estimated. As discussed above the vapour pressure drop budget was

2008 JINST 3 P07003

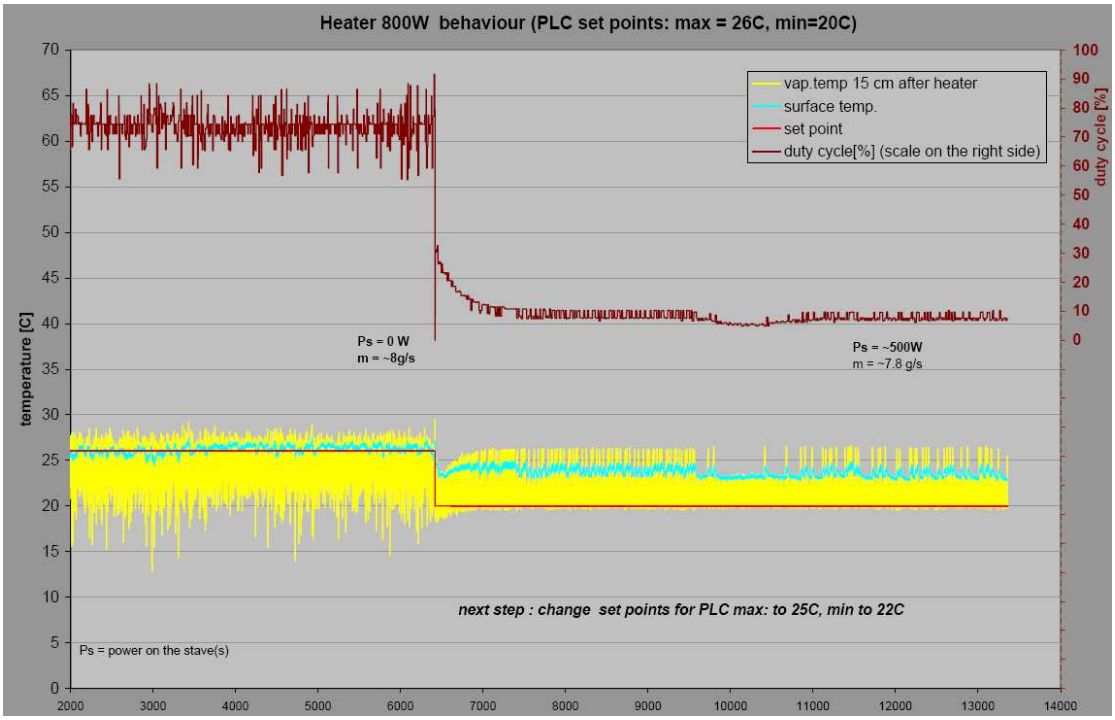

Figure 21. Test of barrel SCT heater: transient from 0 to 100% power on the detector. The heater duty cycle changes from approximately 80% to 7% of the maximum power. The temperature change is smooth and the control is stable. The temperature of the exhaust tube is within the specified range.

limited to 350 mbar for the return, measured from the end of the cooling loop to the back pressure regulator on the cooling racks within the ATLAS cavern. The pressure drop budget for the liquid inlet from the pressure regulator on the cooling racks to the input of the capillary after the heat exchanger was 1 bar. The pressure drops over the long, almost straight, sections of the liquid inlet and vapour return pipe work between the distribution racks and the inner detector volume were estimated from a limited number of measurements and the dependence given in equation (6.1) was assumed for both the liquid and vapour phase:

$$\Delta P = \Delta P_{\mathrm{REF}} \times (ID_{\mathrm{REF}}/ID)^4 \times (L/L_{\mathrm{REF}}) \times (m/m_{\mathrm{REF}})^2 \tag{6.1}$$

where ΔP is the pressure drop, ID the pipe inner diameter, L the pipe length, and m the mass flow through the pipe. All variables followed by $_{\mathrm{REF}}$ refer to the reference measurements used to obtain the pressure drop of the pipe in question.

The total pressure drop budget was split among the individual items, however in some cases hereafter discussed it was not possible to meet the specifications for some of the components due to the space limitations.

The inlet budget is met by all the sub-systems except for the SCT end-cap that has a large pressure drop in the coiled liquid inlet line of the HEX, which is 1000 mbar of the estimated total 1125 mbar pressure drop. Conversely for the Pixel sub-system the inlet pressure drop is dominated by the off-detector pipe work between the cooling racks and the HEX, making up $\sim$70% of the total pressure drop.

2008 JINST 3 P07003

The outlet pressure drop is within specification for the end-cap and Pixel sub-systems, both of which are estimated to be 320 mbar. The end-cap is approximately divided equally 1/3 between the on-cylinder pipe work (which is a worse case estimate), the heater and HEX systems, and the pipe work from the end of the heater to the rack, while the Pixel sub-system is dominated (2/3 of total) by the pressure drop in the pipe work between the detector and the HEX. The SCT barrel sub-system has an estimated pressure drop of 527 mbar, which is in excess of the budget of 350 mbar. This is dominated by the pressure drops of the fluid in the HEX and the heater, which are both approximately 160 mbar. There is also a 90 mbar pressure drop in the barrel sub-system measured between the end of the connector on the cooling manifold and the HEX. The pressure drops over the rest of the barrel off-detector system have been reduced as much as possible with the use of the largest ID pipes that fit into the system.

6.2 On-detector loops

The pressure drops over the on-detector cooling system's staves or cooling loops were measured for a range of C_3F_8 mass flows (controlled by the input pressure of the fluid before the capillary), liquid temperature before the HEX and detector power loads. The pressure drops over the SCT end-cap on-disk pipe work and manifolds were measure to be 330 mbar for the outer cooling loop and 180 mbar for the middle cooling loop for nominal operating conditions. For the worse case, the outer cooling loop, the pressure drop of 330 mbar implies a maximum evaporation pressure of 2 bar absolute, which corresponds to an evaporation temperature in the structure of -20 °C. For a reduced power of 7.5 W per module, the pressure drop falls to 285 mbar, which corresponds to a maximum evaporation temperature of -21 °C. The pressure drop across the SCT barrel cooling loop, including; the barrel 6 manifold with an outlet at 45 degrees to the plane of the manifold, and the connector with a 90 degree bend to connect the manifold to the HEX, is even worse than for the end-cap. The worse case pressure drop, measured at 820 mbar, occurs for the nominal operating conditions, (a power of 504 W, 35 °C inlet liquid temperature and a mass flow of 7.8 g/s). This corresponds to a maximum evaporation temperature increase due to the on-detector cooling structures of 10 °C. This again is an upper limit as extra pipe connections were used in the measurement which increases the pressure drop over the installed cooling loop. However the pressure drop is split over the cooling loop and the manifold and connector; which were deduced from the temperature profile over the on-detector cooling structure, to consist of 540 mbar over the loop (corresponding to a temperature difference from one end of the cooling loop to the other of approximately 6 °C) and 280 mbar over the manifold and connector. As the detector power or the inlet liquid temperature to the HEX is reduced the pressure drop across the HEX is reduced due to a fall in the vapour quality before the cooling structure. Similarly, for a given vapour quality, reducing the mass flow leads to a reduction in the pressure drop over the on-detector cooling structure. Figure 22 and figure 23 show the same pressure drop data measured over the cooling loop and the manifold plus connector as a function of either the detector power or the vapour quality at the outlet of the cooling loop respectively; measured for nominal liquid input parameters and standard capillaries.

The change in outlet vapour quality was obtained by changing the detector power only, while the fluids external conditions were maintained. As can been seen the pressure drop increases with detector power as more of the fluid in the cooling loop is boiled, which is shown as an increase

2008 JINST 3 P07003

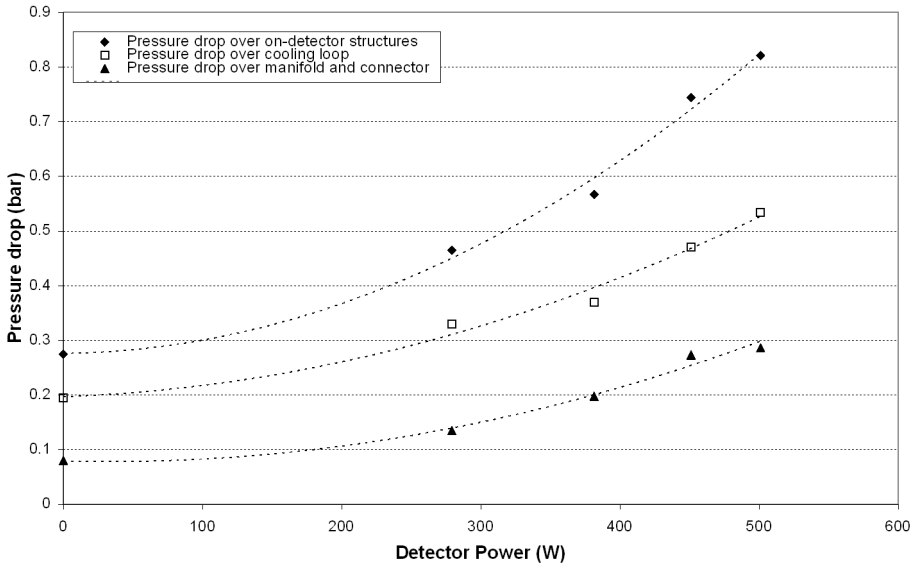

Figure 22. Pressure drop measured over the SCT barrel on-detector structures as a function of detector power, measured at nominal fluid pressures and input liquid temperature. The lines are just to guide the eye.

in vapour quality in figure 23. It is possible to reduce the vapour quality by reducing the inlet liquid temperature before the HEX. At nominal detector power and fluid pressures a reduction in the input liquid temperature to 20 °C results in a reduction in the inlet vapour quality to the cooling loop from 0.38 to 0.15, with a corresponding fall in outlet vapour quality from 0.98 to 0.78.

The pressure drop over the on-detector structures falls from 820 mbar to 650 mbar which corresponds to an evaporation temperature increase due to the on-detector structures of 7.5 °C.

Therefore, assuming realistically an inlet temperature at the heat exchanger of 20 °C, in the case of the SCT barrel the space limitations outside the detector volume lead to a maximum evaporation temperature of −22 °C instead of the −25 °C design target at the exhaust manifold and a maximum evaporation temperature in the barrel 6 on-detector loop of −15.5 °C, due to the additional 7.5 °C worst case increase along the on-detector loop due to the geometry of the detector.

7. System commissioning

The SCT barrel HEX system was tested in the ATLAS ID to measure the system performance before final installation. One quadrant of 5 complete SCT barrel on-detector cooling loops was installed with production capillaries and HEXs. The detector load was simulated by vapour return heaters, controlled by a modified PLC code to allow the power to be set directly. The mechanical interface to the thermal enclosure bulkhead of the barrel was modelled accurately to enable a test of the installation procedure. The system was tested for both warm (evaporation temperature of +13 °C and pressure of 4.8 bar absolute) and cold (evaporation temperature of −18 °C and pressure of 1.9 bar absolute) operation. Due to a problem with the BPRs, since rectified, a lower evaporation temperature was not possible. The inlet liquid temperature to the HEX was not controlled and

2008 JINST 3 P07003

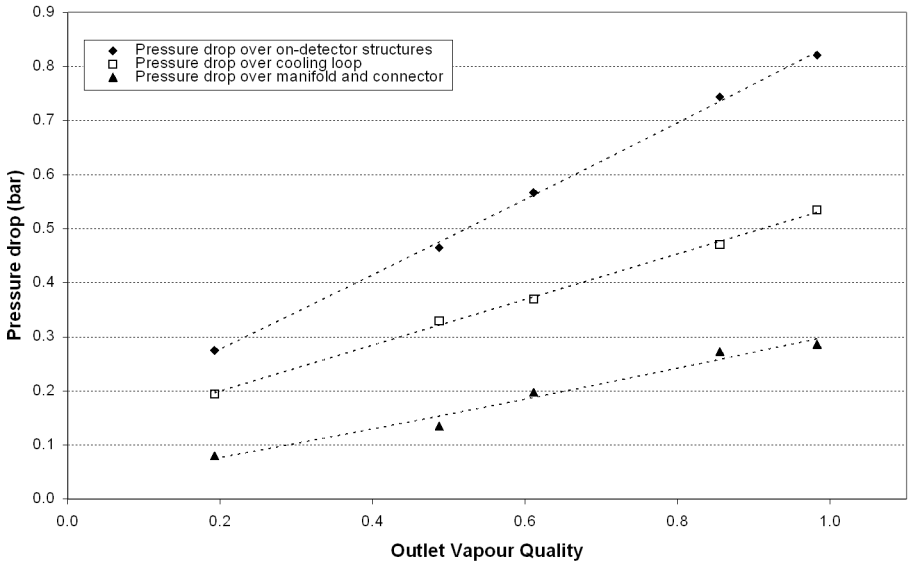

Figure 23. Pressure drop measured over the SCT barrel on-detector structures as a function of vapour quality at the outlet of the cooling loop, measured at nominal fluid characteristics. The lines are just to guide the eye.

was approximately 17 °C, as the external heat load from the system was low because the ATLAS experiment was off.

Further commissioning tests were preformed on all the loops of the SCT and Pixel evaporative system with the use of a screen and copper capillary assembly; with the capillaries sized to supply the correct mass flow with an inlet liquid temperature of 22 °C. The assembly connected the inlet directly to the return vapour heaters. These tests enabled the performance of the compressor/condenser station, the racks, the heater system and the DCS cooling project to be fully tested for all the cooling loops.

7.1 Barrel commissioning measurements

The system was shown to be able to cool the full detector load (504 W) for both cold and warm operation, with a liquid inlet temperature of 17 °C. The closed packed arrangement was shown not to introduce any adverse crosstalk effects onto the operation of the HEXs. The heater's requested power was however, affected by a change in the operational state of its neighbours, but this was not a serious operational problem. The control set-point of the heaters was found to be dependent upon the evaporation temperature of the fluid. The PLC code was modified to take this into account so that it switches automatically between two set-points depending upon the BPR set-point. The final DCS monitoring of the system was shown to work correctly.

The response time from turning on a cooling loop was fast with the fluid cooling the off-detector structures in less than 5 minutes, while the heater obtained stable operation in 15 minutes.

For full detector power and cold operation the average HEX efficiency was 89% with a sub-cooled liquid temperature after the HEX/before the capillary of -12 °C compared to 90% and -17 °C from the laboratory tests measured with a liquid inlet temperature of 20 °C. These are in

2008 JINST 3 P07003

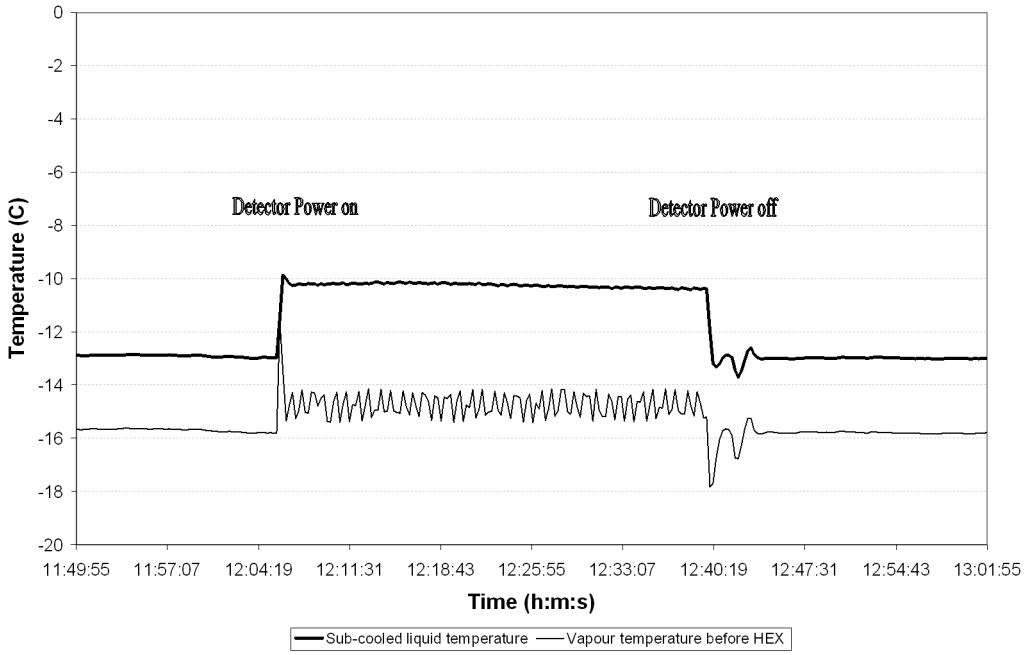

Figure 24. An example of the system temperatures during detector power load cycling for the ATLAS tests of the SCT barrel cooling loops.

reasonable agreement when differences in inlet temperature, evaporation temperature and system insulation are taken into account. As expected, the higher sub-cooled inlet liquid temperature reduced the mass flow slightly from that measured in the laboratory. The heater's duty cycle was approximately 20% for full power and increased to 90% when the detector load was turned off. The duty cycle is high, as expected, for this condition, which represents the maximum mass flow expected in the system.

An extra DCS system was installed during these tests for the purpose of monitoring the pressure drops over the system. The pressure drop from the vapour inlet of the HEX to the BPR on the rack was measured and shown, for full detector power in cold operation, to be in the range 250 to 380 mbar, which is consistent with the extrapolations from the laboratory tests.

The system was shown to be stable to sudden power cycling of the detector load from 0 to 100% of nominal power. Figure 24 shows the vapour temperature before the HEX, which corresponds to the evaporation temperature in the detector load. This increases marginally during powered periods due to the extra pressure drop in the system, the ripple is due to the switched nature of the dummy load power supply. The drop in efficiency of the HEX for the detector-on state is observed in the rise in the sub-cooling inlet liquid temperature, also shown on figure 24.

The system was shown to be robust to a sudden turn off of the compressors of the cooling plant due to a failure. During this failure mode the PLC closes the PRs and BPRs on the rack and flow ceases. The fluid redistributes itself in the system to arrive to saturation conditions throughout, which corresponds to 7 bar absolute at 18 °C, as illustrated in figure 25. The return vapour heater control system regulates downwards the requested power so that the vapour temperature is

2008 JINST 3 P07003

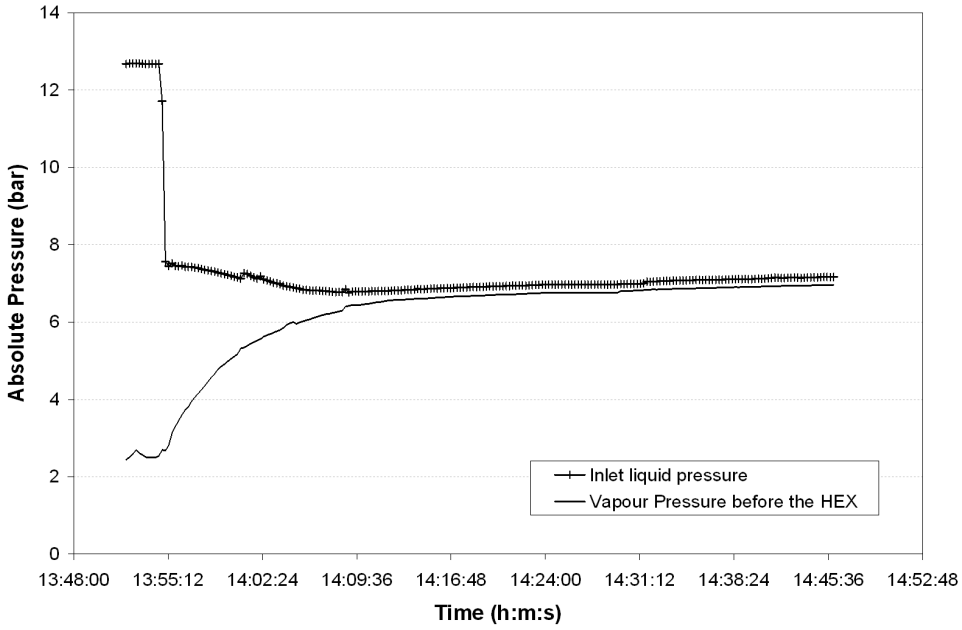

Figure 25. Pressures inside the cooling system as a function of time after a compressor failure.

never excessive, until the heater power requested is constantly low, at which point the PLC turns the heater off.

8. Conclusions

The fundamental design of the ID evaporative cooling, based on a standard industrial direct expansion cooling system, is finished. The system is designed to be as simple and robust as possible to minimise maintenance while being as low mass as possible to reduce material in the tracker volume and in front of the calorimeters. All of the components of the system have been prototyped, tested on an evaporative system in the laboratory with a subset tested in the ATLAS ID. As far as possible, they have been shown to work for the full range of operating conditions expected during the lifetime of the ATLAS experiment. Some of the pressure drops, most notably in the vapour lines of the SCT barrel, are higher than the design requirements due to the limited space and the geometrical constraints. However, this will not affect the operation of the tracker until significant radiation damage has occurred after several years of operation. After then possible system upgrades might be investigated at the level of the off-detector components of the system, as the inner detector can not be altered.

References

[1] ATLAS collaboration, *The ATLAS Detector and Physics Performance: Technical Design Report*, CERN-LHCC-99-014.

2008 JINST 3 P07003

[2] LHC Study Group, T.S. Pettersson and P. Lefévre eds., *The LHC Conceptual Design Report — The Yellow Book,* CERN-AC-95-05 LHC.

[3] ATLAS collaboration, *ATLAS Inner Detector Technical Design Report, vol. 1 and 2,* CERN-LHCC-97-016, CERN-LHCC-97-017.

[4] ATLAS collaboration, *ATLAS Central Solenoid Technical Design Report,* CERN-LHCC-97-21.

[5] M. Olcese et al., *Ultra-light and stable composite structure to support and cool the ATLAS pixel detector barrel electronics modules, Nucl. Instrum. Meth.* **A 518** (2004) 728.

[6] A. Abdesselam et al., *The ATLAS semiconductor tracker end-cap module, Nucl. Instrum. Meth.* **A 575** (2007) 353.

[7] A. Ahmad, *The silicon microstrip sensors of the ATLAS semiconductor tracker, Nucl. Instrum. Meth.* **A 578** (2007) 98.

[8] G. Aad et al., *ATLAS Pixel Detector Electronics and Sensors*, to be published in JINST.

[9] V. Vacek, et al., *Perfluorocarbons and their use in cooling systems for semiconductor particle detectors, Fluid Phase Equilibria* **174** (2000) 191.

[10] V. Vacek, et al., *Velocity of sound measurements in gaseous per fluorocarbons and their mixtures, Fluid Phase Equilibria* **185** (2001) 305.

[11] G. Hallewell, *Evaporative cooling with light fluorocarbons,* presentation at *ATLAS High Luminosity Upgrade Tracker Workshop,* Liverpool, December 6–8 2006.

[12] E. Anderssen et al., *Fluorocarbon evaporative cooling developments for the ATLAS Pixel and Semiconductor tracking detectors*, in *Proceedings of* 5th *Workshop on Electronics for LHC Experiments (LEB99),* Snowmass, Colorado U.S.A. (1999), CERN-OPEN-2000-093, ATLAS-INDET-99-016.

[13] C. Bayer et al., *Development of fluorocarbon evaporative cooling recirculators and controls for the ATLAS Pixel and Semiconductor tracking detectors*, in *Proceedings of* 6th *Workshop on Electronics for LHC Experiments*, Cracow, Poland (2000), http://cdsweb.cern.ch/record/479700.

[14] V. Vacek and V. Vins, *A study of the flow through capillary tubes tuned for a cooling circuit with saturated fluorocarbon refrigerants, Int. J. Thermophys.* **28** (2007) 1490.

2008 JINST 3 P07003